2016-07-01

Computational Studies on Mechanisms and Reactivity of Mercury and Cobalt Organometallic Reactions

Jack Terrell Fuller
Brigham Young University

Computational Studies on Mechanisms and Reactivity of Mercury and Cobalt Organometallic Reactions

Jack Terrell Fuller III

A thesis submitted to the faculty of
Brigham Young University
in partial fulfillment of the requirements for the degree of

Master of Science

Daniel H. Ess, Chair
Roger G. Harrison
Jeremy A. Johnson

Department of Chemistry and Biochemistry

Brigham Young University

July 2016

ABSTRACT

Computational Studies on Mechanisms and Reactivity of
Mercury and Cobalt Organometallic Reactions

Jack Terrell Fuller III
Department of Chemistry and Biochemistry, BYU
Master of Science

Density Functional Theory (DFT) is a powerful tool for treating large organometallic structures efficiently and accurately. DFT calculations on the Hg-catalyzed oxidation of methane to methyl bisulfate in sulfuric acid suggest the lowest energy pathway involves a closed-shell electrophilic C–H activation mechanism coupled with metal alkyl reductive functionalization and oxidation by SO_3. Comparison to Tl, Zn, and Cd suggests that Hg is unique in its ability to catalyze this set of reaction steps. Comparison to $K_2S_2O_8$ highlights the selectivity of this C–H activation reaction as opposed to radical conditions. In contrast, DFT calculations indicate that $Co^{III}(TFA)_3$ oxidizes methane through a radical TFA ligand decarboxylation pathway. A similar decarboxylation pathway is identified for $Mn^{III}(TFA)_3$, but the low spin ground state of $Tl^{III}(TFA)_3$ favors electrophilic C–H activation over this decarboxylation pathway. DFT calculations indicate that $Cp(PPh_2Me)Co{=}CF_2$ undergoes [2 + 2] cycloaddition with TFE by a unique open-shell singlet diradical mechanism. The significant stability of the perfluorometallacyclobutane reveals why catalytic metathesis with TFE is difficult.

Keywords: DFT, mercury, cobalt, C–H activation, decarboxylation, tetrafluoroethylene

ACKNOWLEDGEMENTS

I have received funding during several semesters from Chevron Phillips Chemical Company, LLC, for which I am grateful.

I need to acknowledge my advisor, Dr. Ess. He has helped me accomplish more than I thought I could. I also need to acknowledge Dr. Harrison and Dr. Johnson for their patience and help. My co-workers have also been a great support. Finally, I need to acknowledge my parents and God for all they have done.

Chapter 2 was reproduced in part with permission from: Fuller, J. T., III; Butler, S.; Devarajan, D.; Jacobs, A.; Hashiguchi, B. G.; Konnick, M. M.; Goddard, W. A., III; Gonzales, J.; Periana, R. A.; Ess, D. H. *ACS Catal.* [Online Early Access]. DOI: 10.1021/acscatal.6b00226. Published Online: June 8, 2016. http://pubs.acs.org/doi/pdf/10.1021/acscatal.6b00226 (accessed June 30, 2016). Copyright 2016 American Chemical Society.

Chapter 3 was reproduced in part with permission from: Gustafson, S. J.; Fuller, J. T., III; Devarajan, D.; Snyder, J.; Periana, R. A.; Hashiguchi, B. J.; Konnick, M. M.; Ess, D. H. *Organometallics,* **2015,** *34,* 5485–5495. DOI: 10.1021/acs.organomet.5b00849. Copyright 2015 American Chemical Society.

Chapter 4 was reproduced in part with permission from: Fuller, J. T.; Harrison, D. J.; Leclerc, M. C.; Baker, R. T.; Ess, D. H.; Hughes, R. P. *Organometallics* **2015,** *34,* 5210–5213. DOI: 10.1021/acs.organomet.5b00863. Copyright 2015 American Chemical Society.

TABLE OF CONTENTS

LIST OF SCHEMES

LIST OF FIGURES

1 COMPUTATIONAL METHODS

1.1 Introduction

Density functional theory (DFT) provides a balance of computational efficiency and accuracy in calculating molecular energies and structures.[1] For this reason DFT is particularly useful for studying mechanisms and reactivity in organometallic reactions.

In contrast to accurate *ab initio* methods such as CASPT and CCSD(T), which utilize a wavefunction to describe all electronic interactions, DFT theory uses a ground-state electron density to directly calculate the total electronic energy.[1] The Hohenberg–Kohn theorem states that the ground-state density of a system determines the Hamiltonian and therefore the wavefunctions and energy eigenvalues of a system.[2] This provides the rationale that a unique electron density maps directly to a unique electronic energy. Importantly, DFT is variational and therefore a trial density will always have an associated energy value greater than or equal to the exact energy of a system.

A challenge in DFT is that the exact functional that maps electron densities to energies is unknown.[1] However, Kohn–Sham (KS) theory[3] provides a way to approximate the energy from a given density expressed in terms of KS orbitals. These orbitals are used to calculate the kinetic and potential energies of electrons with no electron-electron repulsion. A classical charge density repulsion term is added along with an approximate exchange-correlation term. The particular

form of the exchange-correlation term determines the physical features built into each density functional and its accuracy.

The following chapter presents brief details of current density functionals and computational methods used in later chapters to examine organometallic reactions.

1.2 Density Functionals

Current DFT functionals can be divided into a hierarchy.[1,4,5] On the lowest rung is the local density approximation (LDA) or local spin density approximation (LSDA). In the LSDA, the exchange and correlation energy terms are functionals of only the α and β spin densities. The second rung comprises generalized gradient approximations (GGAs) and nonseparable gradient approximations (NGAs). Examples include BP86 and BLYP. In these functionals, the exchange and correlation terms depend on both the spin densities and the reduced density gradients. The third rung includes meta-GGAs, such as TPSS and τ-HCTH. These functionals include an additional dependence on the kinetic energy density. On the fourth rung are hybrid meta-GGA functionals that mix a percentage of exact Hartree-Fock (HF) exchange with local exchange. Examples include the often-used B3LYP as well as PBE0 and TPSSh. Currently there are two common classes of hybrid functionals, global and rang-separated, depending on whether the percentage of HF exchange is constant or varies as a function of distance. Functionals on the first three rungs are classified as local, and functionals of the fourth rung are termed nonlocal or hybrid.

The M06 functionals used in subsequent chapters are part of the third and fourth rungs as pure and hybrid meta-GGAs. The M06-L functional is a pure meta-GGA reported in 2006 by Zhao and Truhlar.[6] The exchange-correlation functional includes 37 parameters optimized for 314 data, including atomization energies, ionization potentials, electron and proton affinities,

barrier heights, noncovalent interactions, metal-metal and metal-ligand bond energies, alkyl bond dissociation energies, and isomeric energy differences. The M06-L method was tested against 22 energetic databases that included thermochemistry, kinetics, noncovalent interactions, bond energies, and excitation energies. Compared to eleven local and three hybrid functionals, including B3LYP, M06-L showed the best overall performance, especially for transition metals.

Zhao and Truhlar also developed the M06 functional.[4] The M06 functional is a hybrid meta-GGA functional that includes 27 percent of exact HF exchange. It includes 36 parameters optimized for the same 314 data as M06-L. The M06 functional was tested using a diverse database of 496 energetic and structural data. Compared to 15 other functionals, M06 showed the best overall performance. Therefore, M06 and M06-L are highly recommended for modeling organometallic systems.

1.3 Basis Sets

In practice, KS orbitals and the total electron density are generally constructed using a basis set.[7] Two types of functions generally used in basis sets are Slater-type orbitals (STOs) and Gaussian functions. STOs are advantageous in that they are very similar to atomic orbitals, and therefore fewer can be used to construct accurate orbitals or densities. However, the integrals over multiple STOs involved in calculations have no analytical solutions, so expensive numerical methods must be used. In contrast, Gaussian-type orbitals (GTOs) require more Gaussian functions to represent similarly accurate orbitals, but analytical solutions to integrals greatly speed up calculations. For this reason, GTOs are almost always used.

Gaussian functions are typically contracted to form GTO basis sets. Several Gaussian functions are combined using optimized coefficients to form new functions that more closely resemble atomic orbitals.[7] This leaves fewer coefficients to optimize with DFT but also limits the

flexibility in what the basis set can represent. Because core orbitals typically change much less than valence orbitals, basis functions for core orbitals are usually more contracted than those for valence orbitals. Often only valence orbitals have multiple basis functions, which leads to the terminology n-ζ-valence or valence n-ζ where n is double, triple, etc. indicating the number of contracted functions corresponding to each valence orbital.

Similar to wavefunction methods, larger basis sets in DFT calculations require longer computational times than smaller ones.[7] For transition metals with many electrons, the use of an all electron basis set remains generally impractical for routine calculations, such as geometry optimizations. In addition, core electrons of heavy atoms often demonstrate significant relativistic effects. Therefore, pseudopotentials are often used to decrease the number of electrons treated explicitly. These functions replace nuclear point charges and some or all core electrons with fixed potentials that reproduce the effects of replaced particles on outer electrons. An additional advantage of pseudopotentials is that relativistic effects can be included in their design.

In DFT an increasingly larger basis set usually leads to greater accuracy.[7] Therefore, a computationally advantageous strategy is to calculate stationary points (minima and transition states) using density functionals combined with medium sized basis sets and then to calculate the electronic energies of these structures using large basis sets. This strategy is successful because typically geometries are less sensitive to basis set size than energies. In the studies presented, two medium-sized basis sets are commonly used. The 6-31G(d,p) basis set[8] is used for light atoms such as H, C, O, N, and F, while the LANL2DZ basis set/pseudopotential[9] is used for transition metals.

The 6-31G(d,p) basis set is a valence-double-ζ (or split-valence) Gaussian-type basis set with added polarization functions.[7,8] Polarization functions have larger angular momentum quantum numbers than atomic valence orbitals to allow for greater orbital flexibility, which is crucial for representing chemical bonding.

The def2-TZV class[10] of basis sets is used for electronic energies in the following studies. Weigend and Ahlrichs[10a] first reported these triple-ζ-valence basis sets for elements H through Rn. These basis sets were tested against 311 compounds containing almost all of the elements H through Rn in most of their common oxidation states. Weigend and Ahlrichs reported that the def2-TZVP basis set, which includes polarization functions, achieved small errors close to the DFT basis set limit. Def2-TZVPP results indicated that accuracy improved with additional polarization functions. Rappoport and Furche[10b] later added diffuse functions to form the def2-TZVPD and def2-TZVPPD basis sets. Diffuse functions are necessary for modeling anions and structures with weakly bound electrons.

1.4 Continuum Solvation Models

Solvation effects can be critical for accuracy in modeling organometallic reactions.[11] However, due to the size of organometallic systems and the frequent use of non-aqueous solvents, complete explicit solvation is not practical. Therefore, the studies presented here use continuum (implicit) solvent models. Continuum models at varying levels of sophistication treat the solute explicitly and the solvent as a dielectric medium.

Marenich, Cramer, and Truhlar[12] reported the SMD (solvent model density) continuum solvation model. This model uses the integral-equation-formalism[13] of the polarizable continuum model[14] to solve for bulk electrostatic effects employing the quantum mechanical charge density of the solute. The model adds cavitation, dispersion, and solvent structure effects using atomic

surface tensions. The parameterization of this solvent model included 2821 solvation and transfer free energies in 92 different solvents. Importantly, the parameterization was carried out to allow for the extension of the model to solvents not included in the parameterization. The parameters were organized so that several key macroscopic properties, such as the dielectric constant, radius of solvation, and index of refraction, serve as input parameters for each solvent, and all other parameters remain constant. It was therefore termed a universal solvation model and is particularly useful for modeling less common solvents.

1.5 Summary

DFT is a powerful tool for treating large organometallic structures efficiently and accurately. Two functionals in particular, M06 and M06-L, perform well for organometallic systems. Coupled with continuum solvation models and efficient basis sets, these functionals are used in the following studies.

1.6 References

1. Cramer, C. J. *Essentials of Computational Chemistry*, 2nd ed.; John Wiley & Sons: Chichester, England, 2004; pp 249–303.
2. Hohenberg, P.; Kohn, W. *Phys. Rev.* **1964,** *136,* B864–B871.
3. Kohn, W.; Sham, L. J. *Phys. Rev.* **1965,** *140,* A1133–A1138.
4. Zhao, Y.; Truhlar, D. G. *Theor. Chem. Acc.* **2008,** *120,* 215–241.
5. Yu, H. S.; He, X.; Li, S. L.; Truhlar, D. G. *Chem. Sci.* [Online Early Access]. DOI: 10.1039/C6SC00705H. Published Online: April 6, 2016. http://pubs.rsc.org/en/content/articlepdf/2016/sc/c6sc00705h (accessed June 7, 2016).
6. Zhao, Y.; Truhlar, D. G. *J. Chem. Phys.* **2006,** *125,* 194101.
7. Cramer, C. J. *Essentials of Computational Chemistry*, 2nd ed.; John Wiley & Sons: Chichester, England, 2004; pp 166–180.

8. a) Hariharan, P. C.; Pople, J. A. *Theor. Chim. Acta* **1973,** *28,* 213–222. b) Francl, M. M.; Pietro, W. J.; Hehre, W. J.; Binkley, J. S.; Gordon, M. S.; DeFrees, D. J.; Pople, J. A. *J. Chem. Phys.* **1982,** *77,* 3654–3665.

9. a) Hay, P. J.; Wadt, W. R. *J. Chem. Phys.* **1985,** *82,* 270–283. b) Hay, P. J.; Wadt, W. R. *J. Chem. Phys.* **1985,** *82,* 299–310.

10. a) Weigend, F.; Ahlrichs, R. *Phys. Chem. Chem. Phys.* **2005,** *7,* 3297–3305. b) Rappoport, D.; Furche, F. *J. Chem. Phys.* **2010,** *133,* No. 134105.

11. Cramer, C. J. *Essentials of Computational Chemistry*, 2nd ed.; John Wiley & Sons: Chichester, England, 2004; pp 385–427.

12. Marenich, A. V.; Cramer, C. J.; Truhlar, D. G. *J. Phys. Chem. B* **2009,** *113,* 6378–6396.

13. a) Cancés, E.; Mennucci, B.; Tomasi, J. *J. Chem. Phys.* **1997,** *107,* 3032–3041. b) Mennucci, B.; Cancés, E.; Tomasi, J. *J. Phys. Chem. B.* **1997,** *101,* 10506–10517.

14. a) Miertuš, S.; Scrocco, E.; Tomasi, *J. Chem. Phys.* **1981,** *55,* 117–129. b) Miertuš, S.; Tomasi, *J. Chem. Phys.* **1982,** *65,* 239–245. c) Mennucci, B.; Tomasi, J. *J. Chem. Phys.* **1997,** *106,* 5151–5158. d) Cossi, M.; Scalmani, G.; Rega, N.; Barone, V. *J. Chem. Phys.* **2002,** *117,* 43–54.

2 CATALYTIC MECHANISM OF METHANE OXIDATION BY MERCURY(II) IN SULFURIC ACID

2.1 Introduction

The direct conversion of alkanes to upgraded materials could be an important strategy for decreasing energy usage and CO_2 emissions.[1] However, the homogeneous catalytic functionalization of unactivated alkanes to alcohols remains an unsolved challenge.[2] The C–H σ-bonds of alkanes have large bond dissociation energies (105 kcal/mol for methane) and low acidity and are relatively inert.[3–5] In addition, hydroxylation of one C–H bond in an alkane results in a much more reactive substrate compared to the alkane. One promising strategy that has not yet been commercialized is the use of the C–H activation reaction. In this reaction, a metal-ligand complex generates a metal-alky organometallic intermediate that is subsequently functionalized (Scheme 2-1).

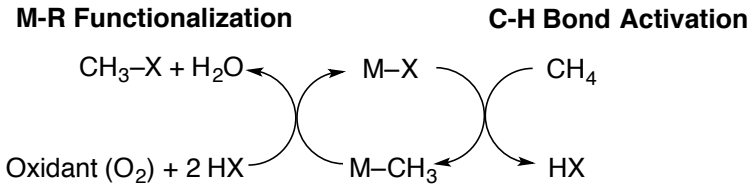

Scheme 2-1: Mechanism of the C–H activation reaction.

Here C–H activation is defined as breaking a C–H bond and forming a metal–carbon bond without forming radicals, carbocations, or carbanions. Shilov and co-workers[4,6] demonstrated C–H activation of alkanes in 1969. Since then, several studies have demonstrated

alkane oxidation by C–H activation.[2,4,7] The most efficient homogeneous alkane oxidation catalysts have been reported by Periana and co-workers[7] using Pt, I, and Hg in concentrated H_2SO_4. While details of the Pt/H_2SO_4 catalytic system are known,[3,8–17] the complete catalytic details of the Hg/H_2SO_4 system have not been reported.[5,18,19]

Periana and co-workers reported the selective oxidation of methane to methyl bisulfate catalyzed by Hg/H_2SO_4 in 1993 (Scheme 2-2).[20] Periana and co-workers proposed a C–H activation and functionalization mechanism that was supported by direct NMR observation of methyl mercuric bisulfate formed at low steady-state concentrations. Additionally, this monomethyl mercury species was synthesized by protonation of dimethyl mercury in sulfuric acid. Deuterium incorporation into methane when catalysis was run in deuterated sulfuric acid suggested that C–H activation was semi-reversible. Radical-type mechanisms were discounted by Periana and co-workers based on the assumption that radical intermediates would result in large amounts of methane overoxidation.

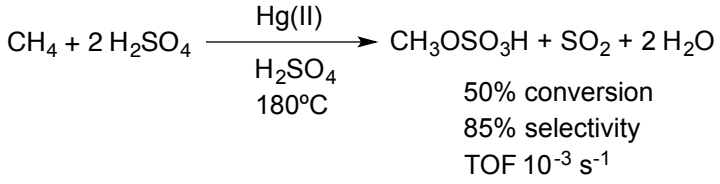

Scheme 2-2: Selective oxidation of methane to methanol catalyzed by Hg^{II} reported by Periana and co-workers.[20]

However, Sen and co-workers subsequently suggested that under some conditions Hg^{II} promoted methane oxidation by an outersphere electron transfer (ET) or radical-initiated mechanism.[21–23] The ET mechanism begins with formation of Hg^{I} radical anion and methane

radical cation (Scheme 2-3b, red arrows). After ET, proton transfer between methane radical cation and bisulfate leads to formation of methyl radical that can be captured by Hg^{I}, giving the same $(HSO_4)Hg^{II}(CH_3)$ intermediate proposed in the C–H activation pathway. There is also the possibility that methyl radical is oxidized to methyl cation and then captured by bisulfate or sulfuric acid. While outersphere ET could be reasonable, proton-coupled electron transfer (PCET) would be more viable given the mismatch of the Hg^{II} reduction potential and methane ionization energy (Scheme 2-3c, orange arrow). PCET would lead directly to the methyl radical intermediate.

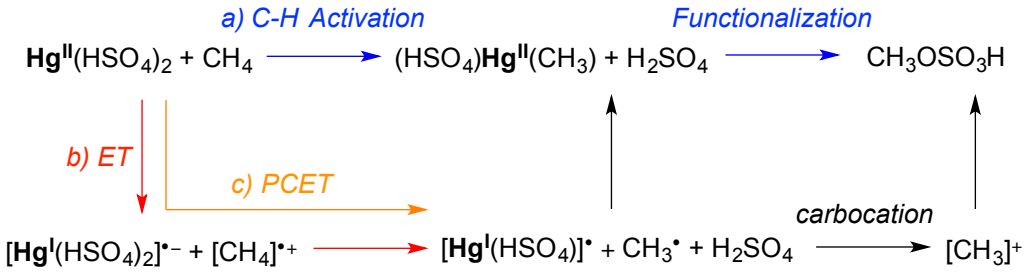

Scheme 2-3: Outline of a) C–H bond activation, b) ET , and c) PCET mechanisms for Hg^{II} catalysis.

In a 1994 report, Sen and co-workers carried out methane oxidation in 98 percent sulfuric acid using $Hg(SO_4)$ at 180 ºC with the predominant product being methyl bisulfate.[21] At 150 ºC the major product was $(HSO_4)Hg^{II}(CH_3)$ with a minor methyl bisulfate product. While these results were consistent with a C–H activation/MR functionalization mechanism, Sen and co-workers proposed ET and radical-initiated mechanisms because other one-electron and two-electron oxidants, such as $K_2S_2O_8$, under conditions where reduced Hg cannot be oxidized resulted in comparable stoichiometric yields of methyl bisulfate. More important, oxidation of

ethane by $Hg(SO_4)$ resulted in formation of up to 25% yield of methyl bisulfate, which suggested C–C bond fragmentation since Hg^{II}-promoted C–C bond activation was considered unlikely. The other product of ethane oxidation was isethionic acid ($HO_3SCH_2CH_2OSO_3H$), which was proposed to result from conversion of ethyl bisulfate to ethylene and oxidation by SO_3.

In a subsequent 1996 report, Sen and co-workers proposed a radical-initiated alkane functionalization mechanism.[22] In this report, methane oxidation with $Hg^{II}(SO_4)$ in fuming sulfuric acid at 160 ºC resulted in a ~3:2 ratio of methanesulfonic acid (CH_3SO_3H) to methyl bisulfate. The use of $K_2S_2O_8$ to oxidize methane resulted in only CH_3SO_3H at 90 ºC and methyl bisulfate at 160 ºC. Sen and co-workers pointed out that while CH_3SO_3H is favored at 90 ºC it is quantitatively converted to methyl bisulfate by heating to 160 ºC in sulfuric acid. In the proposed radical-initiated mechanism, reaction of the initiator and methane forms a methyl radical that combines with SO_3 to give the $CH_3SO_3^{\bullet}$ radical, which subsequently propagates by reacting with methane. Methyl bisulfate forms as the subsequent thermodynamic product.

This chapter presents a density functional theory (DFT) study of both closed-shell and open-shell mechanisms for the selective oxidation of methane to methyl bisulfate catalyzed by Hg^{II}. The complete catalytic cycle is outlined, and comparisons to other d^{10} metal systems and the $K_2S_2O_8$ system are presented. Calculations support a closed-shell electrophilic C–H activation mechanism coupled with reductive functionalization and oxidation by SO_3.

2.2 Computational Details

All calculations were performed using DFT in Gaussian 09[24]. The M06 functional was used due to its demonstrated accuracy for organometallic systems.[25] Geometries were optimized and free energy corrections were calculated using the cc-pwCVDZ-PP[26] basis set and pseudopotential for metal atoms and the aug-cc-pVDZ[27] basis set for non-metal atoms.

Electronic energies were then calculated using M06/def2-TZVPPD.[28] The cc-pwCVDZ-PP basis set and pseudopotential were used for Hg and Tl in particular because it was shown that smaller effective core potentials were necessary to calculate accurate atomic ionization energies.[29] All energies reported in this chapter are free energies. Implicit solvation was included for both geometry optimizations and electronic energy calculations using the SMD model[30] for water with the dielectric constant and radius of solvation modified for 98 percent H_2SO_4 (ε = 98.0, solvent radius = 2.205 Å).[10–16] No dielectric temperature corrections were considered. 3-D figures were rendered using Chemcraft[31].

2.3 Results and Discussion

The starting $Hg^{II}(SO_4)$ complex has the potential to be converted to several new species in sulfuric acid. In solution, the $Hg^{II}(HSO_4)_2$ complex is 12.3 kcal/mol lower in free energy than $Hg^{II}(SO_4)$. Ligand dissociation to form $[Hg^{II}(HSO_4)]^+$ from $Hg^{II}(HSO_4)_2$ is endergonic by 6.0 kcal/mol. However, addition of two explicit solvent molecules changes this ligand dissociation energy estimate to –0.9 kcal/mol. Therefore, it is necessary to examine pathways with neutral and monocationic Hg complexes.

The C–C bond cleavage observed by Sen and co-workers and the similar results when known radical initiators were used led to the proposal that Hg promotes an open-shell alkane oxidation mechanism.[21,22] Thermodynamics of potential open-shell mechanisms are shown in Scheme 2-4. ET between $Hg^{II}(HSO_4)_2$ and CH_4 requires 92.4 kcal/mol. PCET is much more favorable with ΔG = 47.1 kcal/mol, however, it is still less favorable than other mechanisms (see below). Dissociation of one or both bisulfate ligands prior to ET or PCET makes these pathways more favorable. However, it is likely that the implicit solvation model understabilizes these highly charged species. Therefore, these calculations must be interpreted with caution.

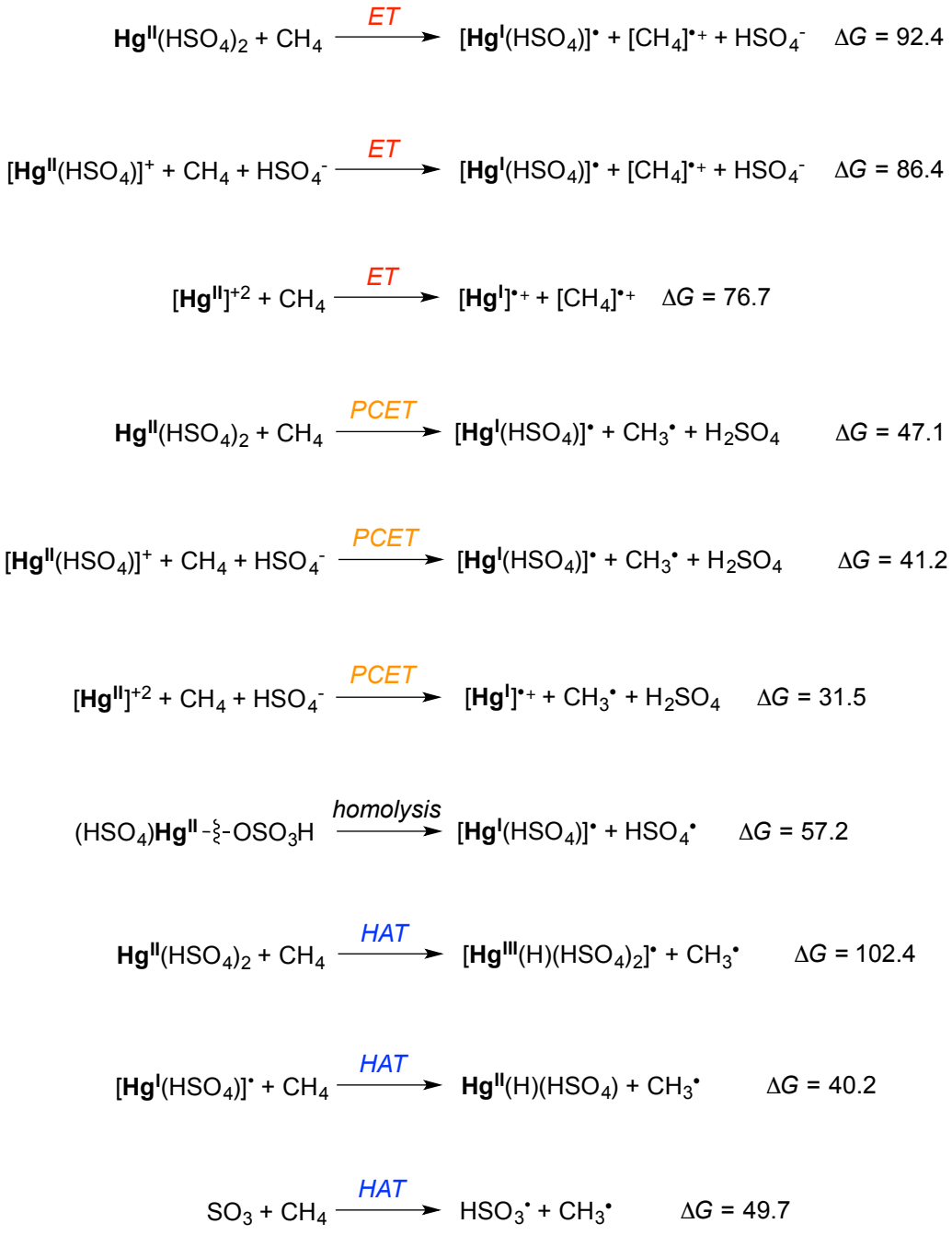

Scheme 2-4: Thermodynamics of open-shell mechanisms considered in this study (kcal/mol).

Bond homolysis that could initiate open-shell pathways is endergonic by 57.2 kcal/mol. Hydrogen atom transfer (HAT) forming $(HSO_4)_2Hg^{III}(H)$ and $H_3C\bullet$ was endergonic by >100 kcal/mol. Even if $Hg^{I}(HSO_4)$ were present in significant concentrations, formation of $(HSO_4)Hg^{II}(H)$ and $H_3C\bullet$ requires 40.2 kcal/mol. HAT with SO_3 is endergonic by 49.7 kcal/mol. All of these open-shell pathways are higher in energy than closed-shell pathways presented below.

Closed-shell mechanisms considered include C–H activation by oxidative addition and by electrophilic substitution. Superacids have been proposed to activate methane[4] through protonation of methane to form $[CH_5]^+$. However, formation of $[CH_5]^+$ and $[Hg^{II}(HSO_4)_3]^-$ is endergonic by 50.1 kcal/mol. Protonation of methane was therefore considered unlikely.

Oxidative addition is possible by Hg^0, Hg^I, and Hg^{II} species. Oxidative addition between methane and $Hg^{II}(HSO_4)_2$, which involves d-electrons, is endergonic by >100 kcal/mol. Oxidative addition with $Hg^{I}(HSO_4)$ is endergonic by 44.8 kcal/mol. Oxidative addition of methane with Hg^0 is most favorable with ΔG = 33.3 kcal/mol, but this process is symmetry forbidden[32] and the frontside S_N2-like transition state has $\Delta G^{\ddagger}$ = 113.4 kcal/mol.

Possible electrophilic substitution pathways are shown in Scheme 2-5. Key transition states are shown in Figure 2-1. $(HSO_4)Hg^{II}(CH_3)$ is formed by **TS1a** (Scheme 2-5, Panel A). Prior ligand dissociation and methane coordination leads to the outersphere electrophilic substitution transition state **TS1b** (Panel B). Other possible electrophilic substitution transition states are the cationic transition states **TS1c** (Panel B) and **TS1d** (Panel C). **TS1b** has the lowest kinetic barrier with $\Delta G^{\ddagger}$ = 32.6 kcal/mol.

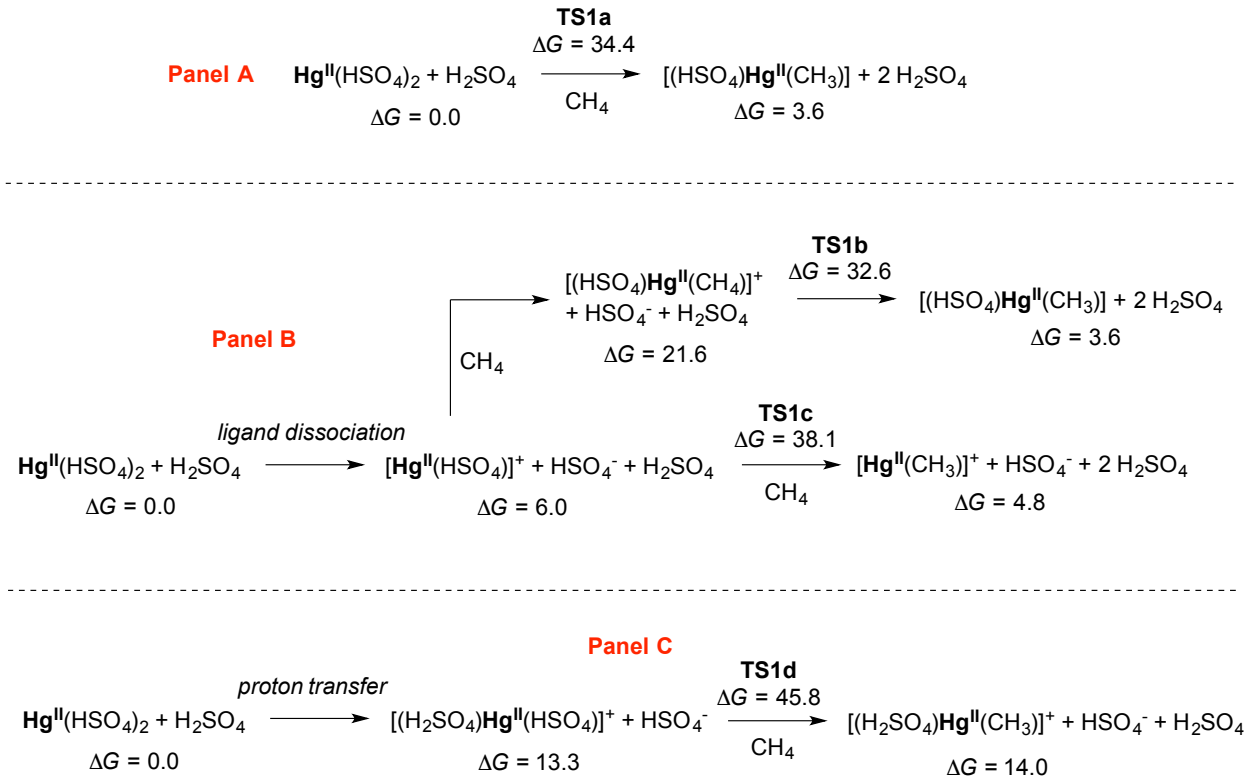

Scheme 2-5: Kinetics and thermodynamics for electrophilic substitution pathways (kcal/mol).

Several functionalization pathways were examined from the $(HSO_4)Hg^{II}(CH_3)$ intermediate. Hg–C bond homolysis is endergonic by 43.5 kcal/mol and heterolysis by 67.8 kcal/mol. Nucleophilic substitution by the bisulfate ligand to form Hg^0 and CH_3OSO_3H is endergonic by only 12.8 kcal/mol. Two transition states were calculated; for the frontside attack similar to reductive elimination $\Delta G^{\ddagger}$ = 57.3 kcal/mol, and for dissociation followed by backside attack $\Delta G^{\ddagger}$ = 34.0 kcal/mol. This backside S_N2 attack (**TS2**) provides the lowest functionalization pathway (Figure 2-2).

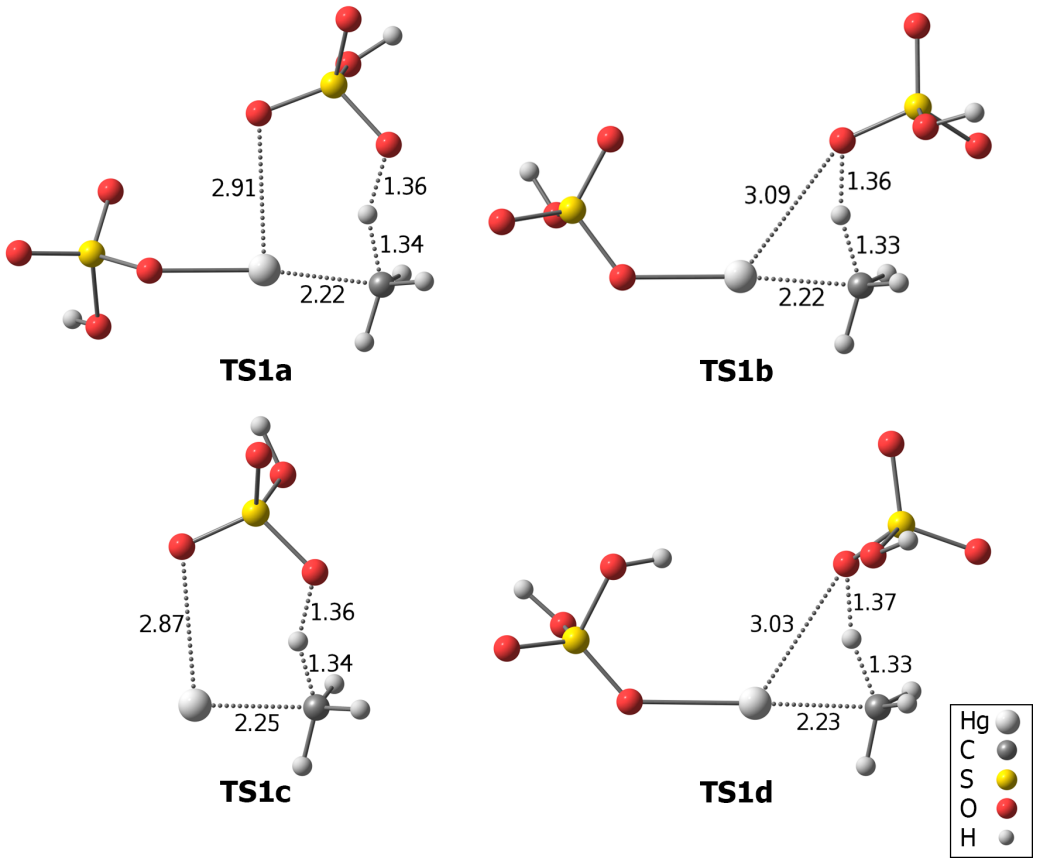

Figure 2-1: Electrophilic substitution transition states (Å).

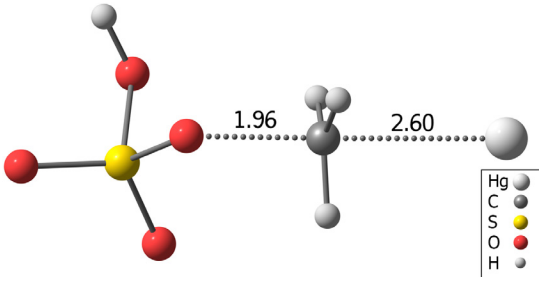

Figure 2-2: Reductive functionalization transition state TS2 (Å).

The products of reductive functionalization are CH_3OSO_3H and Hg^0. Comproportionation of Hg^0 and $Hg^{II}(HSO_4)_2$ to form the binuclear species $[Hg^{I}(HSO_4)]_2$ is exergonic by 25.5

kcal/mol. The complete C–H activation/reductive functionalization energy pathway is shown in Scheme 2-6.

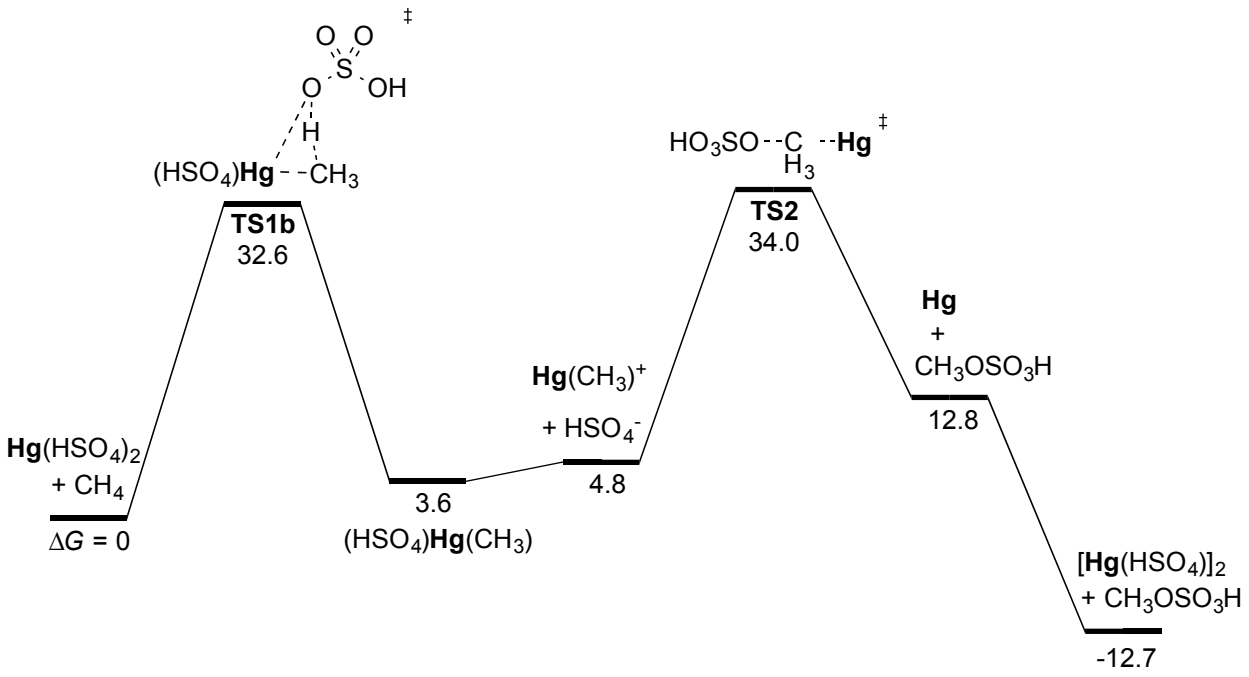

Scheme 2-6: Free energy diagram for complete CH activation/reductive functionalization pathway (kcal/mol).

To test the effects of solvation on the C–H activation/reductive functionalization pathway, one explicit solvent molecule (H_2SO_4) was added to each structure in addition to implicit solvation, and conformations were extensively searched. Several conformations are within ~3 kcal/mol. Importantly, the barriers for C–H activation and reductive functionalization change by less than 1 kcal/mol with inclusion of explicit solvent. This indicates that the continuum solvation model provides a majority of solvation effects. The lowest six conformations for the C–H activation transition state are shown in Figure 2-3.

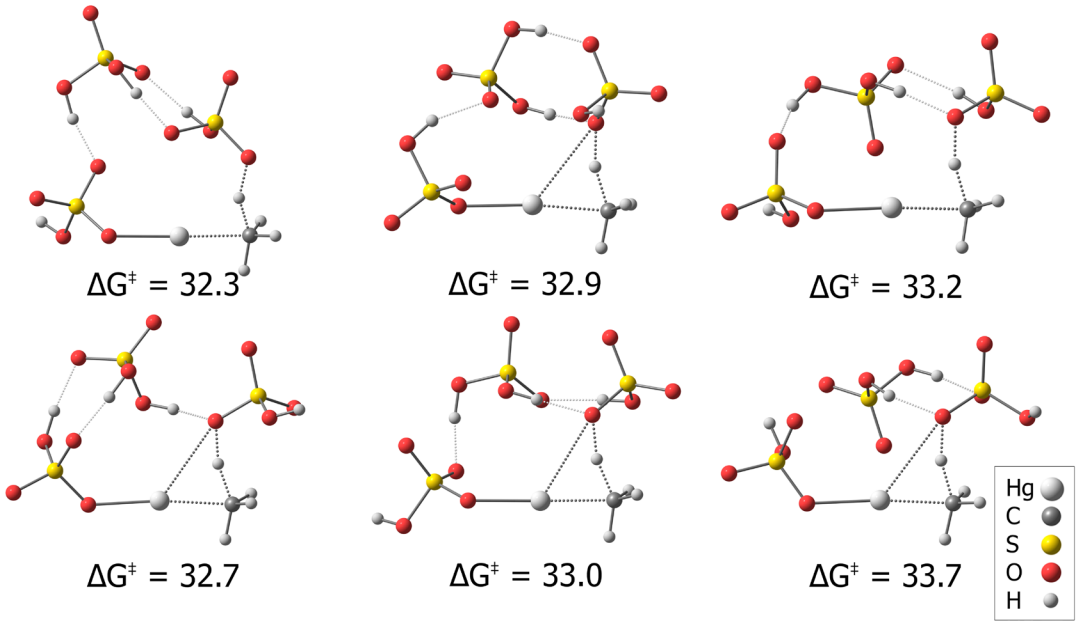

Figure 2-3: C–H activation transition state conformations with mixed explicit/implicit solvation (kcal/mol).

The C–H activation/reductive functionalization pathway energies are consistent with experimental observations. Periana and co-workers[20] observed a low steady-state concentration of $(HSO_4)Hg^{II}(CH_3)$ by NMR. They also observed deuterium incorporation into methane when the reaction was carried out in D_2SO_4. When $(HSO_4)Hg^{II}(CH_3)$ was synthesized and heated to 180 °C, methane and methyl bisulfate were formed. These experimental observations are consistent with an endergonic $(HSO_4)Hg^{II}(CH_3)$ intermediate and the barrier for functionalization slightly higher than the protonolysis barrier (i.e. reverse of C–H activation). In addition, the reaction of Hg^{II} with methane in the non-oxidizing acid CF_3SO_3H formed the Hg^{I} species $[Hg^{I}(CF_3SO_3)]_2$ as well as $CF_3SO_3CH_3$.

The catalytic cycle is completed by oxidation of Hg^{I} to Hg^{II}. The lowest energy pathway involves disproportionation of the Hg^{I} dimer to Hg^{0} and Hg^{II} followed by oxidation of Hg^{0}. The oxidant, SO_3, is present in various concentrations depending on which group carried out the

experimental studies (0 to 33 percent by weight).[20–22] The dehydration of H_2SO_4 to form SO_3 is calculated to be 13.9 kcal/mol endergonic. Therefore, the oxidation pathways were examined with and without the thermodynamic penalty for dehydration.

The energy surface for Hg oxidation is shown in Scheme 2-7 (dehydration penalty included in parentheses). Coordination of SO_3 to Hg^0 is endergonic by 9.8 kcal/mol. This step formally oxidizes Hg^0 to Hg^{II}. Protonation of the sulfonate group and bisulfate coordination forms the $(HSO_4)Hg^{II}(HSO_3)$ intermediate 8.9 kcal/mol higher in energy than Hg^I and SO_3. In the key transition state (**TS3**), solvent protonates the OH group of SO_3H to eject SO_2 and H_2O (Figure 2-4). For this transition state, $\Delta G^{\ddagger}$ = 25.4 kcal/mol.

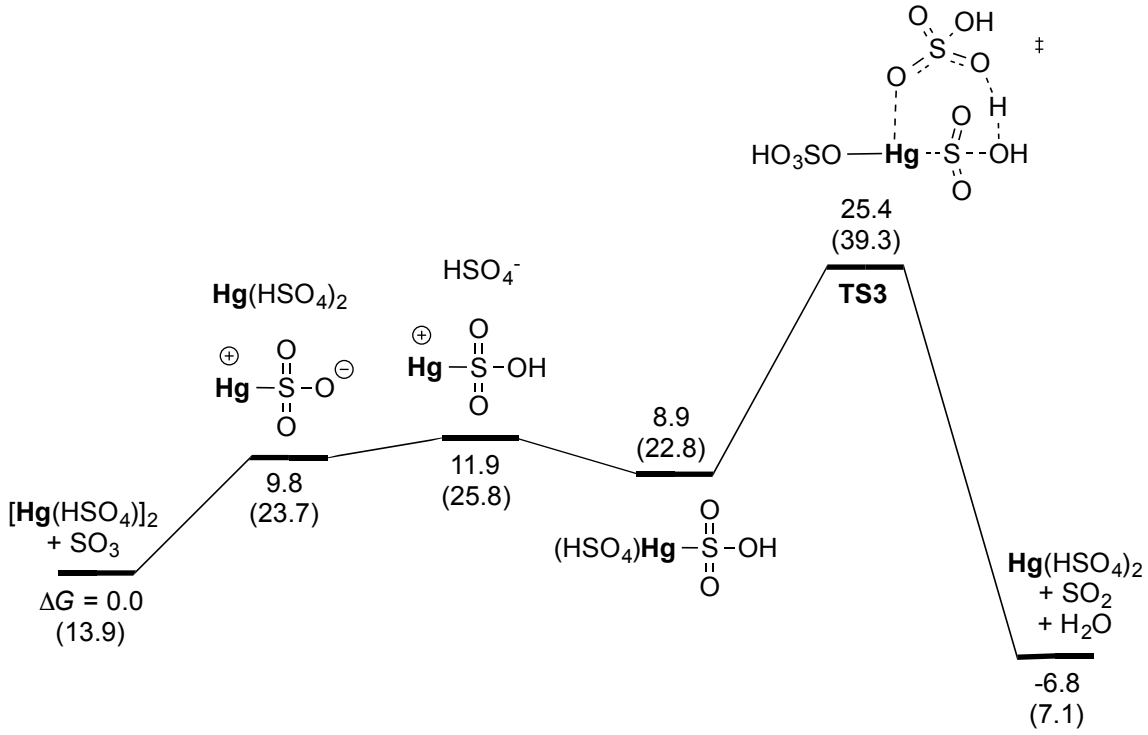

Scheme 2-7: Free energy diagram for oxidation of Hg^I to Hg^{II} by SO_3 (kcal/mol). The penalty for dehydration of H_2SO_4 is included in the values in parentheses.

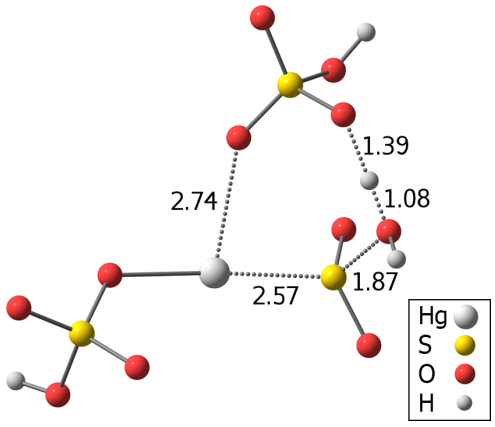

Figure 2-4: Oxidation transition state TS3 (Å).

With the penalty for dehydration of H_2SO_4 included, the oxidation step as well as subsequent C–H activation and reductive functionalization steps have barriers of ~40 kcal/mol. This significant dependence of the barrier heights on the concentration of SO_3 is consistent with the experimental observation that catalysis slows when the concentration of H_2SO_4 drops below ~80 percent.[7] Nevertheless, barriers of ~40 kcal/mol for all three segments of the catalytic cycle suggest that Hg is uniquely efficient in catalyzing electrophilic methane C–H functionalization in sulfuric acid.

The unique nature of Hg in sulfuric acid is also demonstrated by comparison with Tl. Periana and co-workers found that Tl^{III} stoichiometrically oxidized methane to methyl bisulfate in sulfuric acid.[7] Calculated barriers for the C–H activation and reductive functionalization steps are <20 kcal/mol. However, consistent with no observed catalytic turnover, the Tl oxidation transition state analogous to **TS3** has $\Delta G^{\ddagger}$ = 74.7 kcal/mol. This indicates that the Tl^{I} to Tl^{III} potential is too large for turnover with sulfuric acid as the terminal oxidant.

Zn and Cd are congeners of Hg, and because the reduction potentials of these metals are lower than that of Hg it could be assumed that the oxidation barriers would be lower. However,

the reductive functionalization transition states analogous to **TS2** have $\Delta G^{\ddagger} > 70$ kcal/mol. This suggests that Zn and Cd will also not catalyze the reaction.

Sen and co-workers proposed a radical mechanism for the $Hg^{II}(SO_4)$ oxidation of alkanes in part because $K_2S_2O_8$, a known radical initiator,[33] also oxidized methane in concentrated sulfuric acid.[21–23] The calculated mechanism of oxidation by $[S_2O_8]^{2-}$ in fuming sulfuric acid[22] (~30 percent SO_3 by weight) follows a radical chain mechanism as expected (Scheme 2-8).

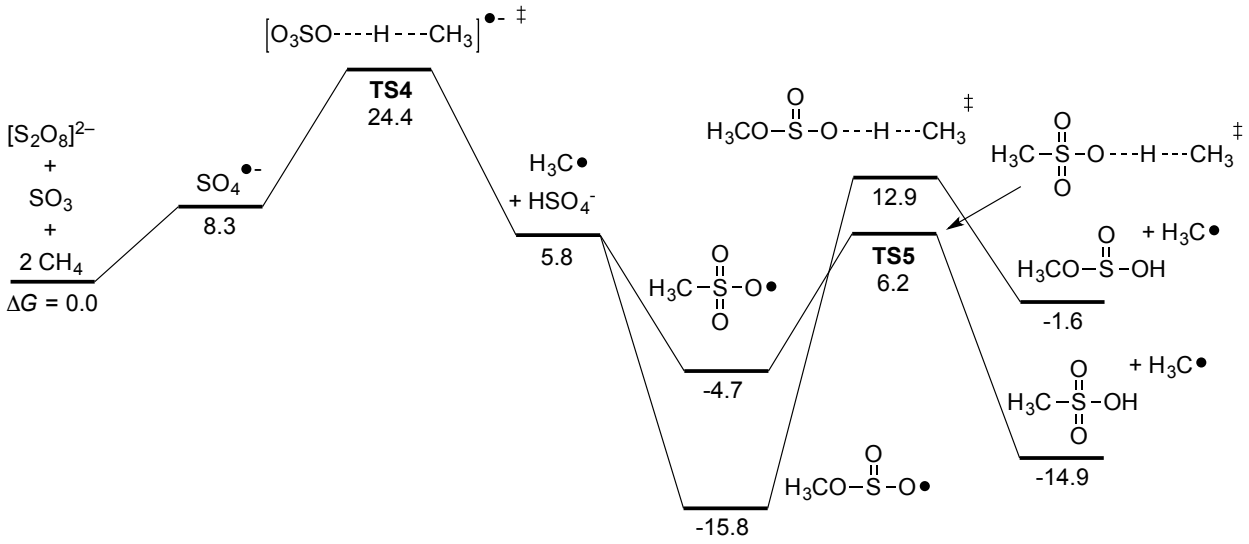

Scheme 2-8: Free energy diagram for radical oxidation of methane by $[S_2O_8]^{2-}$ (kcal/mol).

The reaction is initiated by O–O bond homolysis of $[S_2O_8]^{2-}$, requiring 8.3 kcal/mol. Hydrogen atom abstraction via **TS4** forms methyl radical and bisulfate anion with $\Delta G^{\ddagger} = 24.4$ kcal/mol. C–S bond formation followed by hydrogen atom abstraction via **TS5** is the preferred pathway both thermodynamically and kinetically with $\Delta G^{\ddagger} = 22.0$ kcal/mol.

One assumed advantage of the electrophilic C–H activation mechanism is the prevention of overoxidation. The C–H activation transition state of methyl bisulfate with Hg^{II} has $\Delta G^{\ddagger} =$

42.7 kcal/mol. This is ~10 kcal/mol higher than **TS1b**, indicating high selectivity for methane. In contrast, hydrogen abstraction by CH_3SO_3• favors methane over methyl bisulfate by only 1.4 kcal/mol, suggesting lower selectivity and potential overoxidation.

2.4 Conclusion

DFT calculations on the Hg-catalyzed oxidation of methane to methyl bisulfate in sulfuric acid suggest the lowest energy pathway involves a closed-shell electrophilic C–H activation mechanism coupled with metal alkyl reductive functionalization and oxidation by SO_3. Comparison to Tl, Zn, and Cd suggests that Hg is unique in its ability to catalyze this set of reaction steps. Comparison to $K_2S_2O_8$ highlights the selectivity of this C–H activation reaction as opposed to radical conditions.

2.5 References

1. Ivars, F.; López Nieto, J. M. In *Handbook of Advanced Methods and Processes in Oxidation Catalysis: From Laboratory to Industry*; Duprez, D., Cavani, F., Eds.; Imperial College Press: London, 2014; Chapter 24, pp 767–834.

2. Crabtree, R. H. *J. Chem. Soc., Dalton Trans.*, **2001,** 2437–2450.

3. Ahlquist, M.; Nielsen, R. J.; Periana, R. A.; Goddard, W. A., III. *J. Am. Chem. Soc.* **2009,** *131,* 17110–17115.

4. Shilov, A. E.; Shul'pin, G. B. *Chem. Rev.* **1997,** *97,* 2879–2932.

5. Conley, B. L.; Tenn, W. J., III; Young, K. J. H.; Ganesh, S.; Meier, S.; Ziatdinov, V.; Mironov, O.; Oxgaard, J.; Gonzales, J.; Goddard, W. A., III; Periana, R. A. In *Activation of Small Molecules*; Tolman, W. B., Ed.; WILEY-VCH Verlag GmbH & Co. KGaA: Weinheim, Germany, 2006; Chapter 7, pp 235–285.

6. Shilov, A. E.; Shteinman, A. A. *Coord. Chem. Rev.* **1977,** *24,* 97–143.

7. Hashiguchi, B. G.; Bischof, S. M.; Konnick, M. M.; Periana, R. A. *Acc. Chem. Res.* **2012,** *45,* 885–898.

8. Mylvaganam, K.; Bacskay, G. B.; Hush, N. S. *J. Am. Chem. Soc.* **1999,** *121,* 4633–4639.

9. Mylvaganam, K.; Bacskay, G. B.; Hush, N. S. *J. Am. Chem. Soc.* **2000,** *122,* 2041–2052.

10. Gilbert, T. M.; Hristov, I.; Ziegler, T. *Organometallics* **2001,** *20,* 1183–1189.

11. Kua, J.; Xu, X.; Periana, R. A.; Goddard, W. A., III. *Organometallics* **2002,** *21,* 511–525.

12. Xu, X.; Kua, J.; Periana, R. A.; Goddard, W. A., III. *Organometallics* **2003,** *22,* 2057–2068.

13. Hristov, I. H.; Ziegler, T. *Organometallics* **2003,** *22,* 1668–1674.

14. Xu, X.; Fu, G.; Goddard, W. A., III; Periana, R. A. *Stud. Surf. Sci. Catal.* **2004,** *147,* 499–504.

15. Paul, A.; Musgrave, C. B. *Organometallics* **2007,** *26,* 793–809.

16. Ahlquist, M.; Periana, R. A.; Goddard, W. A., III. *Chem. Commun.* **2009,** 2373–2375.

17. Balcells, D.; Clot, E.; Eisenstein, O. *Chem. Rev.* **2010,** *110,* 749–823.

18. Horsley, J. A.; Vanderveken, D. J.; Periana, R. A. *Catal. Today* **1995,** *23,* 333–339.

19. Cundari, T. R.; Yoshikawa, A. *J. Comput. Chem.* **1998,** *19*, 902–911.

20. Periana, R. A.; Taube, D. J.; Evitt, E. R.; Löffler, D. G.; Wentrcek, P. R.; Voss, G.; Masuda, T. *Science* **1993,** *259,* 340–343.

21. Sen, A.; Benvenuto, M. A.; Lin, M.; Hutson, A. C.; Basickes, N. *J. Am. Chem. Soc.* **1994,** *116,* 998–1003.

22. Basickes, N.; Hogan, T. E.; Sen, A. *J. Am. Chem. Soc.* **1996,** *118,* 13111–13112.

23. Sen, A. *Acc. Chem. Res.* **1998,** *31,* 550–557.

24. Frisch, M. J.; Trucks, G. W.; Schlegel, H. B.; Scuseria, G. E.: Robb, M. A.; Cheeseman, J. R.; Scalmani, G.; Barone, V.; Mennucci, B.; Petersson, G. A.; Nakatsuji, H.; Caricato, M.; Li, X.; Hratchian, H. P.; Izmaylov, A. F.; Bloino, J.; Zheng, G.; Sonnenberg, J. L.; Hada, M.; Ehara, M.; Toyota, K.; Fukuda, R.; Hasegawa, J.; Ishida, M.; Nakajima, T.; Honda, Y.; Kitao, O.; Nakai, H.; Vreven, T.; Montgomery, J. A., Jr.; Peralta, J. E.; Ogliaro, F.; Bearpark, M.; Heyd, J. J.; Brothers, E.; Kudin, K. N.; Staroverov, V. N.; Kobayashi, R.; Normand, J.; Raghavachari, K.; Rendell, A.; Burant, J. C.; Iyengar, S. S.; Tomasi, J.; Cossi, M.; Rega, N.; Millam, J. M.; Klene, M.; Knox, J. E.; Cross, J. B.; Bakken, V.; Adamo, C.; Jaramillo, J.; Gomperts, R.; Stratmann, R. E.; Yazyev, O.; Austin, A. J.; Cammi, R.; Pomelli, C.; Ochterski, J. W.; Martin, R. L.; Morokuma, K.; Zakrzewski, V. G.; Voth, G. A.; Salvador, P.; Dannenberg, J. J.; Dapprich, S.; Daniels, A. D.; Farkas, Ö.; Foresman, J. B.; Ortiz, J. V.; Cioslowski, J.; Fox, D. J. *Gaussian 09, Revision B.01*, Gaussian, Inc., Wallingford CT, USA, 2009.

25. Zhao, Y.; Truhlar, D. G. *Theor. Chem. Acc.* **2008,** *120,* 215–241.

26. a) Figgen, D.; Rauhut, G.; Dolg, M.; Stoll, H. *Chem. Phys.* **2005,** *311,* 227–244. b) Peterson, K. A.; Puzzarini, C. *Theor. Chem. Acc.* **2005,** *114,* 283–296. c) Metz, B.; Schweizer, M.; Stoll, H.; Dolg, M.; Liu, W. *Theor. Chem. Acc.* **2000,** *104,* 2–28. d) Peterson, K. A.; Yousaf, K. E. *J. Chem. Phys.* **2010,** *133,* No. 174116. e) Feller, D. *J. Comp. Chem.* **1996,** *17,* 1571–1586. f) Schuchardt, K. L.; Didier, B. T.; Elsethagen, T.; Sun, L.; Gurumoorthi, V.; Chase, J.; Li, J.; Windus, T. L. *J. Chem. Inf. Model.* **2007,** *47,* 1045–1052.

27. a) Dunning, T. H., Jr. *J. Chem. Phys.* **1989,** *90,* 1007–1023. b) Kendall, R. A.; Dunning, T. H., Jr.; Harrison, R. J. *J. Chem. Phys.* **1992,** *96,* 6796–6806. c) Woon, D. E.; Dunning, T. H., Jr. *J. Chem. Phys.* **1993,** *98,* 1358–1371.

28. a) Weigend, F.; Ahlrichs, R. *Phys. Chem. Chem. Phys.* **2005,** *7,* 3297–3305. b) Rappoport, D.; Furche, F. *J. Chem. Phys.* **2010,** *133,* No. 134105. c) Andrae, D.; Häußermann, U.; Dolg, M.; Stoll, H.; Preuß, H. *Theor. Chim. Acta* **1990,** *77,* 123–141. d) Metz, B.; Schweizer, M.; Stoll, H.; Dolg, M.; Liu, W. *Theor. Chem. Acc.* **2000,** *104,* 2–28. e) Feller, D. *J. Comp. Chem.* **1996,** *17,* 1571–1586. f) Schuchardt, K. L.; Didier, B. T.; Elsethagen, T.; Sun, L.; Gurumoorthi, V.; Chase, J.; Li, J.; Windus, T. L. *J. Chem. Inf. Model.* **2007,** *47,* 1045–1052.

29. Gustafson, S. J.; Fuller, J. T., III; Devarajan, D.; Snyder, J.; Periana, R. A.; Hashiguchi, B. J.; Konnick, M. M.; Ess, D. H. *Organometallics*, **2015,** *34,* 5485–5495.

30. Marenich, A. V.; Cramer, C. J.; Truhlar *J. Phys. Chem. B* **2009,** *113,* 6378–6396.

31. http://www.chemcraftprog.com

32. Wolters, L. P.; van Zeist, W. J.; Bickelhaupt, F. M. *Chem. – Eur. J.* **2014,** *20,* 11370–11381.

33. Lin, M.; Sen, A. *J. Chem. Soc., Chem. Commun.* **1992,** 892–893.

3 MECHANISM OF COBALT(III) TRIFLUOROACETATE PROMOTED METHANE OXIDATION

3.1 Introduction

Over the past several decades most reported examples of activation and functionalization of hydrocarbon C–H bonds involved second-row and third-row transition metal complexes. First-row transition metals have the advantage of low cost and abundance; however, multiple spin states and thus potential radical mechanisms may be a significant drawback. Additionally, mechanistic studies of first-row C–H activation and functionalization reactions are lacking.

Cooper and Waters[1] and later Heiba, Dessau, and Koehl[2] reported an example of first-row transition metal induced oxidation of aromatic C–H bonds. In this case, Co^{III} induced oxidation of aromatic C–H bonds by an electron transfer (ET) step to form a radical cation intermediate that was confirmed by ESR spectroscopy.[2–5] Another example was reported by Jones and Mellor[6,7] who showed that Co^{III} oxidizes C–H bonds of adamantanes but found no evidence for a radical mechanism.

In 1990, Moiseev and co-workers reported that Co^{III} reacts stoichiometrically to partially oxidize methane in trifluoroacetic acid (TFAH) at 180 °C (Scheme 3-1).[8] A 90 percent yield of methyl trifluoroacetate (MeTFA) was generated based on Co^{III}. A significant amount of CO_2 was also reported. Methane oxidation to MeTFA became catalytic in Co when O_2 was added. Additionally, under catalytic conditions there was a high selectivity for MeTFA versus overoxidation products. Whether or not methane is present and with O_2 similar amounts of CO_2 were formed.

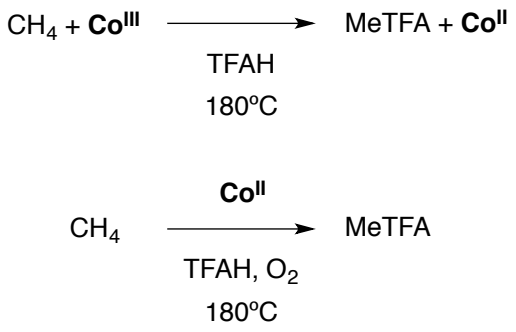

Scheme 3-1: Stoichiometric methane oxidation by Co^{III} and catalytic methane oxidation by Co^{II} in trifluoroacetic acid.[8]

In 1991, Moiseev and co-workers[9] reported the oxidation of ethane and propane by Co^{III}. In this case, there was significant overoxidation, C–C bond cleavage, and formation of CHF_3. Based on this evidence, Moiseev proposed an oxidation mechanism that involved outersphere ET with an alkane radical cation intermediate (Scheme 3-2). This was proposed to lead to C–C and/or C–H bond cleavage and further reaction with O_2 or Co^{III}.

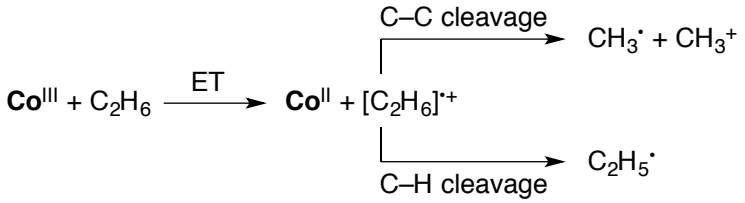

Scheme 3-2: ET mechanism proposed by Moiseev and co-workers.[9]

This chapter reports DFT calculations that compare possible closed-shell C–H activation and open-shell radical pathways for methane oxidation to MeTFA by $Co^{III}(TFA)_3$. Overall, these calculations demonstrate that the high-spin ground state of $Co^{III}(TFA)_3$ provides a low-energy pathway for TFA ligand decarboxylation to stimulate a radical oxidation mechanism.

3.2 Computational Details

All calculations were performed using density functional theory (DFT) in Gaussian 09[10]. M06 and M06-L density functionals used in this study were selected due to their broad accuracy for organometallic systems.[11,12] Additionally, these functionals perform well in calculating bond energies of first-row transition metal compounds[13] as well as spin-state transition energies and ionization potentials for neutral first-row transition metals and their monocations.[14] In this chapter, calculations reported correspond to M06 energies and structures, unless stated otherwise. Geometries were optimized and free energy corrections were calculated using the LANL2DZ basis set and pseudopotential[15] for metal atoms and the 6-31G(d,p) basis set[16] for non-metal atoms. Electronic energies were then calculated using the def2-TZVPD basis set.[17,18] All energies reported are free energies. Implicit solvation was included during geometry optimizations and for electronic energies using the SMD model[19] for water with the dielectric and solvent radius modified for trifluoroacetic acid (ε = 8.42,[20] solvent radius = 2.479 Å). The SMD model accurately reproduces the solvation energy of monocationic metals and the pK_a of trifluoroacetic acid.[21] Minimum energy crossing points (MECPs) were located using MECPro[22] that interfaces with Gaussian 09. 3-D figures were rendered using Chemcraft[23].

3.3 Results and Discussion

The ground state of the d^6 $Co^{III}(TFA)_3$ complex is the quintet spin state, with the singlet and triplet states 8.6 kcal/mol and 8.8 kcal/mol higher in free energy, respectively. M06-L predicts the same ordering of spin states. The relatively small energy difference between spin states indicates the possibility of reaction pathways on multiple spin states with intersystem crossing. For each of these spin states, TFA ligand dissociation to form $[Co^{III}(TFA)_2]^+$ and TFA^-

requires >37 kcal/mol. With inclusion of an explicit solvent dimer, ligand dissociation and solvent coordination to form $[Co^{III}(TFA)_2(TFAH)]^+$ and $[(TFA)(TFAH)]^-$ has $\Delta G > 32$ kcal/mol.

Four general mechanisms were examined (Scheme 3-3): (1) Electrophilic C–H activation/substitution involving formation of a Co–Me intermediate. (2) ET, (3) Hydrogen atom transfer, and (4) Radical decarboxylation.

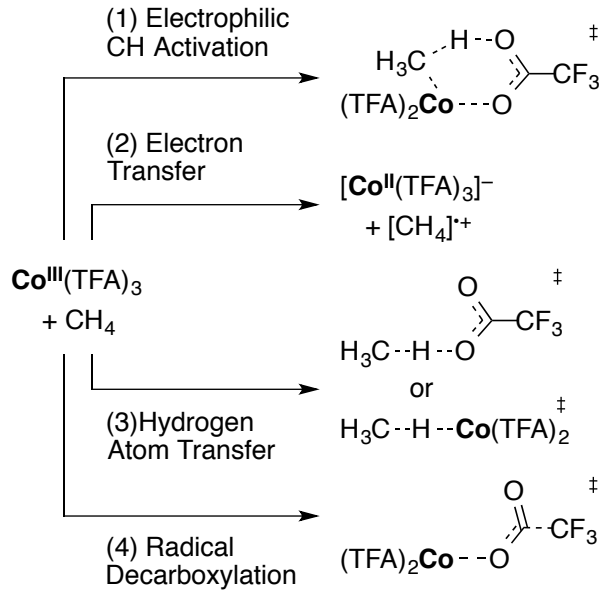

Scheme 3-3: General methane oxidation mechanisms examined.

Electrophilic C–H activation occurs through simultaneous formation of a Co–C bond and deprotonation of methane by a TFA ligand. The lowest energy electrophilic C–H activation transition state is on the quintet energy surface with $\Delta G^{\ddagger} = 33.7$ kcal/mol (Figure 3-1). The C–H activation transition states on the singlet and triplet energy surfaces have $\Delta G^{\ddagger} = 37.4$ kcal/mol and 35.9 kcal/mol, respectively. These C–H activation barriers are not prohibitively high in

energy, and this indicates that C–H functionalization catalysts based on Co^{III} could be important. However, for this case, these C–H activation barriers are higher than other mechanisms.

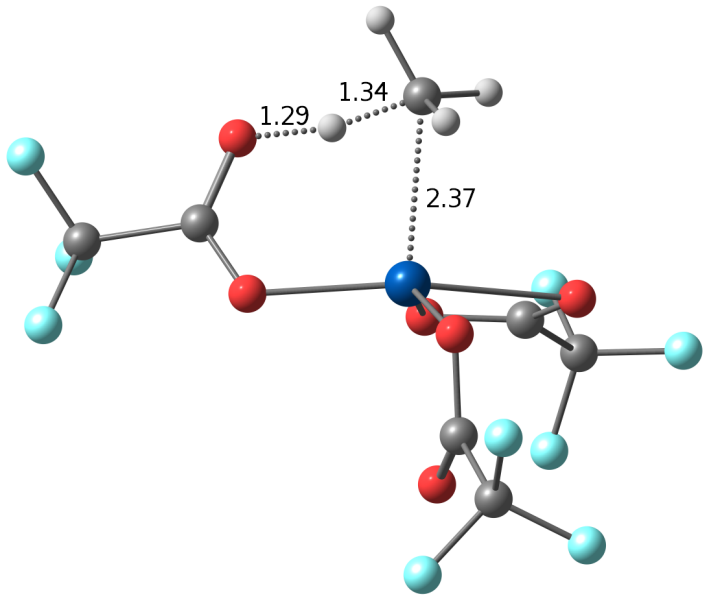

Figure 3-1: Electrophilic C–H Activation transition state (Å).

Outersphere ET is thermodynamically unfavorable. ET between $Co^{III}(TFA)_3$ and CH_4 to form $[Co^{II}(TFA)_3]^{\bullet-}$ and $[CH_4]^{\bullet+}$ is endergonic by 63.7 kcal/mol. The monocationic $[Co^{III}(TFA)_2]^+$ complex is unlikely to be present in significant quantities, and additionally ET between $[Co^{III}(TFA)_2]^+$ and CH_4 is endergonic by 38.8 kcal/mol. This suggests that outersphere ET pathways are unlikely.

Both the Co metal and a TFA ligand can potentially accept a hydrogen atom transferred from methane. However, no stable Co^{IV} hydride was located. Formation of a Co^{III} hydride from $Co^{II}(TFA)_2$ and methane is endergonic by > 80 kcal/mol. Abstraction of hydrogen by a TFA still coordinated to the Co metal center to form $(TFAH)Co^{II}(TFA)_2$ and methyl radical is more

thermodynamically favorable, and $\Delta G^{\ddagger}$ = 33.8 kcal/mol. Co–O bond homolysis to form a TFA radical and $Co^{II}(TFA)_2$ is endergonic by 20.4 kcal/mol, and subsequent hydrogen abstraction from methane has $\Delta G^{\ddagger}$ = 7.7 kcal/mol. This gives a total free energy barrier of 28.1 kcal/mol.

However, the lowest energy pathway identified involves decarboxylation of a TFA ligand (Scheme 3-4). For the decarboxylation of $Co^{III}(TFA)_3$ to form $Co^{II}(TFA)_2$, CO_2, and CF_3•, $\Delta G^{\ddagger}$ = 21.6 kcal/mol on the quintet energy surface. The decarboxylation transition state is lower in energy on the triplet energy surface, and $\Delta G^{\ddagger}$ = 16.8 kcal/mol (Figure 3-2). A MECP between the quintet and triplet spin states exists at 13.0 kcal/mol, which suggests that intersystem crossing to the triplet surface may be facile.[24]

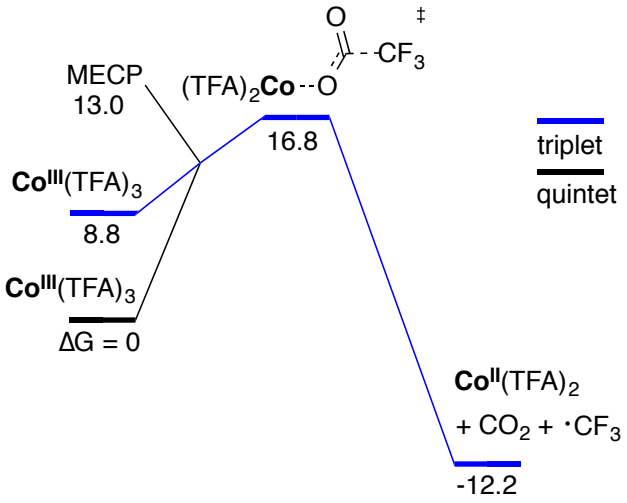

Scheme 3-4: Decarboxylation energy landscape for $Co^{III}(TFA)_3$ (kcal/mol).

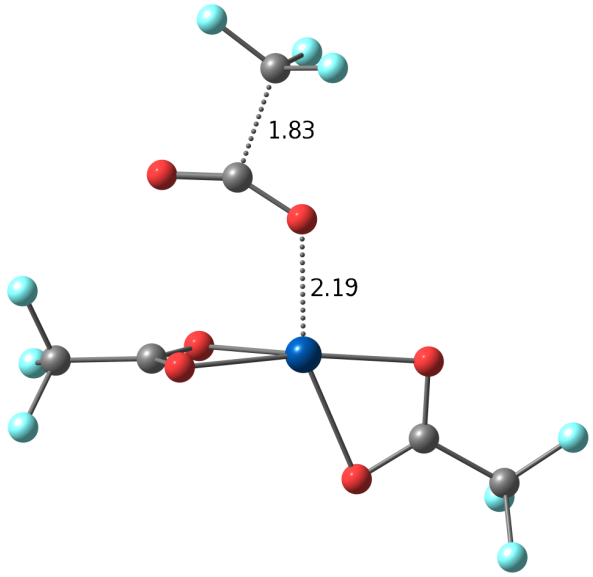

Figure 3-2: Triplet decarboxylation transition state (Å).

This Co-TFA decarboxylation pathway is consistent with the report by Waters and Clifford[25] that Co^{III} salts decarboxylated aliphatic carboxylic acids. Because reactivity increased with increasing α-substitution, Waters and Clifford proposed a rate-determining step that involved direct decarboxylation ("concerted fragmentation") of the cobalt(III) carboxylate complex to form Co^{II}, CO_2, and the alkyl radical. Later experiments by Lande and Kochi[26] supported this proposal.

Decarboxylation is exergonic by 12.2 kcal/mol. CF_3• can further react by abstracting a hydrogen atom from solvent or from methane. Hydrogen atom transfer with TFAH solvent has $\Delta G^{\ddagger}$ = 24.6 kcal/mol. However, hydrogen atom transfer with methane is more favorable with $\Delta G^{\ddagger}$ = 17.4 kcal/mol, forming methyl radical (Scheme 3-5).

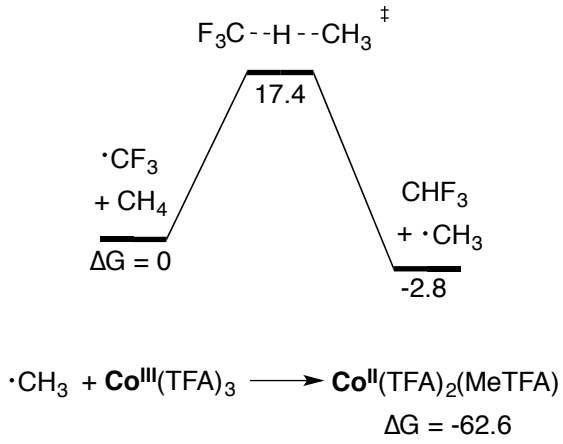

Scheme 3-5: Methane functionalization by CF_3• (kcal/mol).

Methyl radical can then react directly with solvent or with a second equivalent of $Co^{III}(TFA)_3$ to form MeTFA. Formation of [MeTFAH]$^{\bullet}$ has $\Delta G^{\ddagger}$ = 27.6 kcal/mol. As reported above, bond homolysis of $Co^{III}(TFA)_3$ has a barrier of 20.4 kcal/mol, which allows for radical recombination to form MeTFA. However, scans of the addition of methyl radical to $Co^{III}(TFA)_3$ without bond homolysis indicate this reaction has no potential energy barrier. Formation of the $Co^{II}(TFA)_2$MeTFA complex is exergonic by 62.6 kcal/mol (Scheme 3-5). Dissociation of MeTFA, the final product, is further exergonic by ~3 kcal/mol.

Moiseev and co-workers[8] also reported that $Mn^{III}(TFA)_3$ produced a significant amount of MeTFA under similar conditions to Co^{III}. Additionally, the Periana and Ess groups reported that $Tl^{III}(TFA)_3$ oxidized methane to MeTFA in TFAH.[21] Therefore, calculations were carried out to determine if the decarboxylation pathway was viable for $Mn^{III}(TFA)_3$ and $Tl^{III}(TFA)_3$ oxidants.

The ground state of $Mn^{III}(TFA)_3$ is a quintet spin state. The lowest decarboxylation transition state on this surface has $\Delta G^{\ddagger}$ = 21.8 kcal/mol (Scheme 3-6). This suggests that

$Mn^{III}(TFA)_3$, similar to $Co^{III}(TFA)_3$, generates MeTFA by a radical decarboxylation mechanism. The larger decarboxylation barrier for $Mn^{III}(TFA)_3$ compared with $Co^{III}(TFA)_3$ is consistent with a lower MeTFA yield of 30 percent.[8]

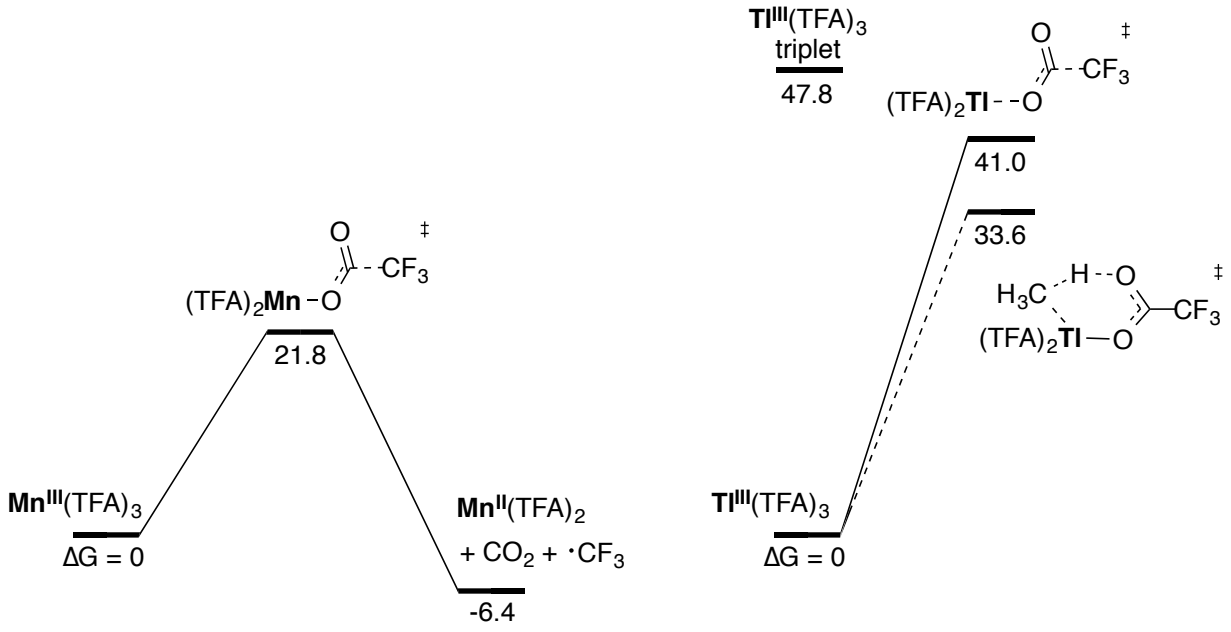

Scheme 3-6: Mn^{III} and Tl^{III} decarboxylation pathways (kcal/mol).

The triplet state of the d^{10} $Tl^{III}(TFA)_3$ is 47.8 kcal/mol higher in energy than the singlet ground state (Scheme 3-6). From the triplet there is no significant barrier to decarboxylation. The open-shell singlet decarboxylation transition state has $\Delta G^{\ddagger}$ = 41.0 kcal/mol, with an S^2 value of 0.9. Despite the significant spin contamination,[27] this transition state indicates that TFA ligand decarboxylation is not possible for $Tl^{III}(TFA)_3$ due to the low spin ground state, and therefore C–H activation is the lowest energy pathway as previously reported.[28]

3.4 Conclusion

DFT calculations reported in this chapter indicate that $Co^{III}(TFA)_3$ oxidizes methane through a radical TFA ligand decarboxylation pathway. A similar decarboxylation pathway was identified for $Mn^{III}(TFA)_3$. In contrast, the low spin ground state of $Tl^{III}(TFA)_3$ disfavors this decarboxylation pathway, and therefore electrophilic C–H activation is the lowest energy pathway for methane oxidation.

3.5 References

1. Cooper, T. A.; Waters, W. A. *J. Chem. Soc. B* **1967,** 687–695.
2. Heiba, E. I.; Dessau, R. M.; Koehl, W. J., Jr. *J. Am. Chem. Soc.* **1969,** *91,* 6830–6837.
3. Dessau, R. M.; Shih, S.; Heiba, E. I. *J. Am. Chem. Soc.* **1970,** *92,* 412–413.
4. Kochi, J. K.; Tang, R. T.; Bernath, T. *J. Am. Chem. Soc.* **1973,** *95,* 7114–7123.
5. Dessau, R. M. *J. Am. Chem. Soc.* **1970,** *92,* 6356–6358.
6. Jones, S. R.; Mellor, J. M. *J. Chem. Soc., Chem. Commun.* **1976,** 385–386.
7. Jones, S. R.; Mellor, J. M. *J. Chem. Soc., Perkin Trans. 2* **1977,** 511–517.
8. Vargaftik, M. N.; Stolarov, I. P.; Moiseev, I. I. *J. Chem. Soc., Chem. Commun.* **1990,** 1049–1050.
9. Stolarov, I. P.; Vargaftik, M. N.; Shishkin, D. I.; Moiseev, I. I. *J. Chem. Soc., Chem. Commun.* **1991,** 938–939.
10. Frisch, M. J.; Trucks, G. W.; Schlegel, H. B.; Scuseria, G. E.: Robb, M. A.; Cheeseman, J. R.; Scalmani, G.; Barone, V.; Mennucci, B.; Petersson, G. A.; Nakatsuji, H.; Caricato, M.; Li, X.; Hratchian, H. P.; Izmaylov, A. F.; Bloino, J.; Zheng, G.; Sonnenberg, J. L.; Hada, M.; Ehara, M.; Toyota, K.; Fukuda, R.; Hasegawa, J.; Ishida, M.; Nakajima, T.; Honda, Y.; Kitao, O.; Nakai, H.; Vreven, T.; Montgomery, J. A., Jr.; Peralta, J. E.; Ogliaro, F.; Bearpark, M.; Heyd, J. J.; Brothers, E.; Kudin, K. N.; Staroverov, V. N.; Kobayashi, R.; Normand, J.; Raghavachari, K.; Rendell, A.; Burant, J. C.; Iyengar, S. S.; Tomasi, J.; Cossi, M.; Rega, N.; Millam, J. M.; Klene, M.; Knox, J. E.; Cross, J. B.; Bakken, V.; Adamo, C.; Jaramillo, J.; Gomperts, R.; Stratmann, R. E.; Yazyev, O.; Austin, A. J.; Cammi, R.; Pomelli, C.; Ochterski, J. W.; Martin, R. L.; Morokuma, K.; Zakrzewski, V. G.; Voth, G. A.; Salvador, P.; Dannenberg, J. J.; Dapprich, S.; Daniels, A. D.; Farkas, Ö.;

Foresman, J. B.; Ortiz, J. V.; Cioslowski, J.; Fox, D. J. *Gaussian 09, Revision B.01*, Gaussian, Inc., Wallingford CT, USA, 2009.

11. Zhao, Y.; Truhlar, D. G. *Theor. Chem. Acc.* **2008,** *120,* 215–241.

12. Zhao, Y.; Truhlar, D. G. *J. Chem. Phys.* **2006,** *125,* 194101.

13. Zhang, W.; Truhlar, D. G.; Tang, M. *J. Chem. Theory Comput.* **2013,** *9,* 3965–3977.

14. Luo, S.; Averkiev, B.; Yang, K. R.; Xu, X.; Truhlar, D. G. *J. Chem. Theory Comput.* **2014,** *10,* 102–121.

15. a) Hariharan, P. C.; Pople, J. A. *Theor. Chim. Acta* **1973,** *28,* 213–222. b) Francl, M. M.; Pietro, W. J.; Hehre, W. J.; Binkley, J. S.; Gordon, M. S.; DeFrees, D. J.; Pople, J. A. *J. Chem. Phys.* **1982,** *77,* 3654–3665.

16. a) Hay, P. J.; Wadt, W. R. *J. Chem. Phys.* **1985,** *82,* 270–283. b) Hay, P. J.; Wadt, W. R. *J. Chem. Phys.* **1985,** *82,* 299–310.

17. a) Weigend, F.; Ahlrichs, R. *Phys. Chem. Chem. Phys.* **2005,** *7,* 3297–3305. b) Rappoport, D.; Furche, F. *J. Chem. Phys.* **2010,** *133,* No. 134105. c) Feller, D. *J. Comp. Chem.* **1996,** *17,* 1571–1586. d) Schuchardt, K. L.; Didier, B. T.; Elsethagen, T.; Sun, L.; Gurumoorthi, V.; Chase, J.; Li, J.; Windus, T. L. *J. Chem. Inf. Model.* **2007,** *47,* 1045–1052.

18. Xu, X.; Truhlar, D. G. *J. Chem. Theory Comput.* **2012,** *8,* 80–90.

19. Marenich, A. V.; Cramer, C. J.; Truhlar *J. Phys. Chem. B* **2009,** *113,* 6378–6396.

20. Dannhauser, W.; Cole, R. H. *J. Am. Chem. Soc.* **1952,** *74,* 6105.

21. Hashiguchi, B. G.; Konnick, M. M.; Bischof, S. M.; Gustafson, S. J.; Devarajan, D.; Gunsalus, N.; Ess, D. H.; Periana, R. A. *Science* **2014,** *343,* 1232–1237.

22. Available for download from D. H. Ess at http://www.chem.byu.edu/faculty/daniel-h-ess/mecp-software-download. Based on program developed by J. N. Harvey, see Harvey, J. N.; Aschi, M.; Schwarz, H.; Koch, W. *Theor. Chem. Acc.* **1998,** *99,* 95–99.

23. http://chemcraftprog.com

24. Harvey, J. N. *Phys. Chem. Chem. Phys.* **2007,** *9,* 331–343.

25. Clifford, A. A.; Waters, W. A. *J. Chem. Soc.* **1965,** 2796–2804.

26. Lande, S. S.; Kochi, J. K. *J. Am. Chem. Soc.* **1968,** *90,* 5196–5207.

27. a) Gräfenstein, J.; Cremer, D. *Mol. Phys.* **2001,** *99,* 981–989. b) Cramer, C. J. *Essentials of Computational Chemistry,* 2nd ed.; John Wiley & Sons: Chichester, England, 2004; pp 565–574.

28. Gustafson, S. J.; Fuller, J. T., III; Devarajan, D.; Snyder, J.; Periana, R. A.; Hashiguchi, B. J.; Konnick, M. M.; Ess, D. H. *Organometallics* **2015,** *34,* 5485–5495.

4 MECHANISM OF [2 + 2] CYCLOADDITION BETWEEN COBALT DIFLUOROCARBENE AND TETRAFLUOROETHYLENE

4.1 Introduction

Alkene metathesis by transition metal carbene complexes is a highly valuable reaction used in polymer synthesis and drug discovery that was recognized with the 2005 Nobel Prize in Chemistry.[1–4] The general mechanism (Chauvin mechanism) involves alkene coordination, [2 + 2] cycloaddition to form a metallacyclobutane, and retro-cycloaddition to form a new metal carbene/alkene pair (Scheme 4-1).

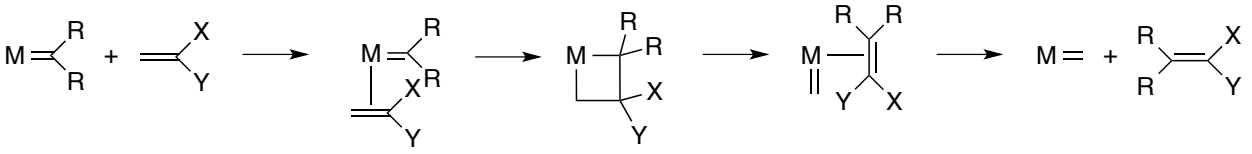

Scheme 4-1: Chauvin mechanism for olefin metathesis.

While catalytic metathesis reactions are very successful with alkenes, catalytic metathesis reactions involving tetrafluoroethylene (TFE) are generally unsuccessful.[5] In 2015, Takahira and Morizawa[6] reported the tetrafluoroethenolysis cross metathesis between TFE and nonfluorinated vinyl ethers in the presence of a Ru-carbene catalyst to produce a difluorinated olefin. In 2013, Baker and co-workers demonstrated that [2 + 2] cycloaddition between the cobalt perfluorocarbene $(Cp)(PPh_2Me)Co{=}CF_2$ (**1**, Scheme 4-2) and TFE after four days at room temperature formed the corresponding perfluorometallacyclobutane (**2**).[7] This non-catalytic reaction demonstrated the viability of rare perfluorometallacyclobutane intermediates.

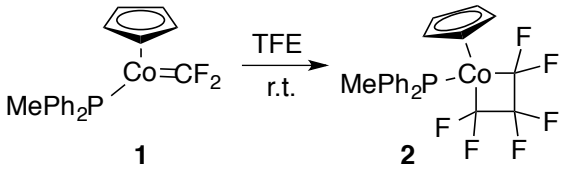

Scheme 4-2: Perfluorometallacyclobutane formation reported by Baker and co-workers[7].

This [2 + 2] cycloaddition reaction is remarkable because complex **1** is coordinatively saturated and it is therefore unclear how a metallacycle can be formed. Alkene coordination does not occur by phosphine dissociation as experimental studies showed that the rate of metallacycle formation is only slightly slower with excess phosphine. This chapter reports density functional calculations that support a unique open-shell stepwise [2 + 2] cycloaddition mechanism involving a singlet diradical intermediate leading to perfluorometallacyclobutane formation from complex (**1**) and TFE.

4.2 Computational Details

Geometries were optimized in Gaussian 09[8] and Jaguar[9] with (U)M06[10]/LACVP**, which combines the 6-31G(d,p) basis set[11] for H, C, F, and P and the LANL2DZ basis set and effective core potential[12] for Co. (U)M06/def2-TZVP[13]//M06/LACVP** was used for electronic energies. Electronic energies include implicit solvation by tetrahydrofuran (THF) using a Poisson-Boltzmann model[14]. Free energies reported use (U)M06/LACVP** thermodynamic corrections. To approximate adiabatic spin-state crossing energies, geometries and energies of minimum energy crossing points (MECPs) were calculated using the Harvey program combined with Gaussian 09 and Jaguar.[15] For open-shell singlet structures, spin projection was used to

generate final energies using the equation: $E^{SP}_{singlet} = E_{singlet} + [<S^2>_{singlet}/(<S^2>_{triplet} - <S^2>_{singlet})](E_{singlet} - E_{triplet})$.[16] 3-D figures were rendered using Chemcraft.[17]

4.3 Results and Discussion

Four general [2 + 2] cycloaddition pathways were explored with calculations (Scheme 4-3). (1) Cp slip: Because the Co is coordinatively saturated, it is possible that TFE coordination occurs after the Cp ligand changes from η^5 to η^3 coordination. (2) Concerted [2 + 2] cycloaddition: Concerted addition can take place after coordination of TFE or directly with complex **1**. (3) Co–C/C–C stepwise cycloaddition: This pathway involves Co–C bond formation to generate a polar or radical intermediate followed by C–C bond rotation and C–C bond formation. (4) C–C/Co–C stepwise cycloaddition: This pathway involves C–C bond formation to generate a polar or radical intermediate followed by C–C bond rotation and Co–C bond formation. For pathways 3 and 4, triplet and singlet spin states are possible for the d^8 Co complex.

Complex **1** has a ground-state singlet spin state with the triplet state 10.9 kcal/mol higher in free energy. The MECP between the singlet and triplet $(Cp)(PPh_2Me)Co{=}CF_2$ complex is 11.4 kcal/mol above the singlet, which suggests possible intersystem crossing. However, the lowest-energy pathway identified does not require spin state crossing (see below).

TFE coordination with η^5 to η^3 Cp coordination change requires ΔG = 35.6 kcal/mol relative to separated **1** and TFE. Without coordination number change at the Co metal center, the concerted [2 + 2] cycloaddition has $\Delta G^{\ddagger}$ > 50 kcal/mol, despite the very favorable thermodynamics with ΔG = -25.3 kcal/mol. This suggests an effectively forbidden, yet irreversible, reaction.

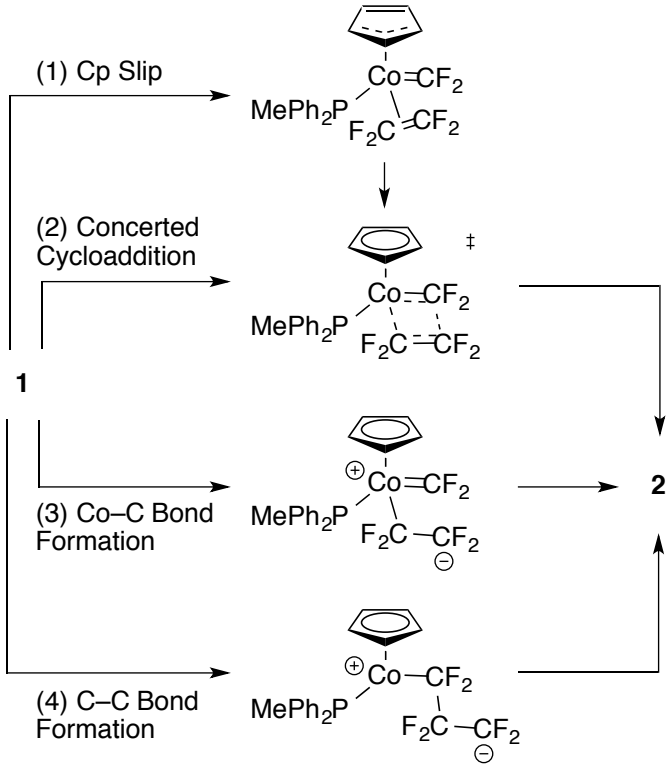

Scheme 4-3: Possible [2 + 2] cycloaddition mechanisms.

Metal fluorocarbenes generally follow the donor/acceptor or singlet model for carbenes.[18] In this model, the metal-carbon bond comprises σ-donation of two electrons from the carbon and π-backbonding of two electrons from the metal. The nucleophilicity or electrophilicity of the carbene depends on how much electron density the metal center donates through π-backbonding. Low-valent metals typically donate more and form nucleophilic fluorocarbenes. Cp and CO ligands compete for back-donation and may make the fluorocarbene electrophilic. For **1**, the PPh_2Me ligand likely increases the nucleophilic character of this metal fluorocarbene. Therefore, forming the C–C bond is endergonic by 26.8 kcal/mol (**3**, Scheme 4-4) while forming the Co–C bond is endergonic by 37.9 kcal/mol (**4**, Scheme 4-4).

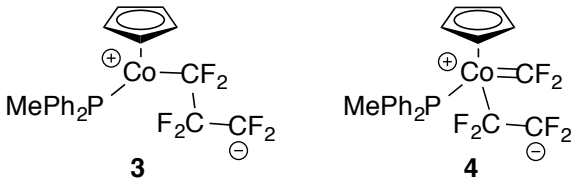

Scheme 4-4: Possible polar intermediates formed during stepwise cycloaddition.

Open-shell singlet and triplet stepwise intermediates are significantly lower in energy than polar intermediates. For example, the open-shell singlet (Cp)(PPh_2Me)Co–$CF_2CF_2CF_2$• has ΔG = 1.1 kcal/mol, and the triplet has ΔG = 1.4 kcal/mol. The open-shell singlet has S^2 = ~1.0, indicating a 50:50 mixture of singlet and triplet states,[19] which is consistent with the nearly degenerate singlet and triplet spin state energies. The C–C bond forming transition state leading to the open-shell singlet intermediate is shown in Figure 4-1.

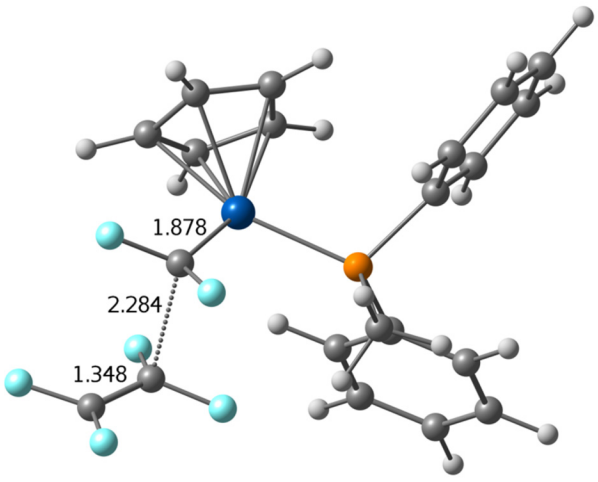

Figure 4-1: Singlet C–C bond forming transition state (Å).

The open-shell singlet C–C transition state has a spin-projected $\Delta G^{\ddagger}$ = 27.8 kcal/mol. The triplet transition state barrier is 29.3 kcal/mol. Because the MECP for **1** is lower than the singlet and triplet barriers for C–C formation these barrier heights are not definitive as to whether only the singlet spin state pathway follows. However, if the triplet transition state does occur as a minor pathway, the resulting (Cp)(PPh_2Me)Co–$CF_2CF_2CF_2$• triplet intermediate must undergo spin state intersystem crossing to form the subsequent Co–C bond. Scheme 4-5 shows the singlet spin free energy landscape for perfluorometallacyclobutane formation. After C–C bond formation (**5**), the energy surface is very flat, and C–C bond rotation occurs with a barrier of ~2 kcal/mol to form **6**. Co–C bond formation has an extremely small barrier of < 1 kcal/mol. The flatness of the energy surface could suggest that after the C–C bond forming transition state the lifetime of open-shell intermediates is governed by dynamics.

Alternative to the mechanisms described in Scheme 4-3, because the Co=CF_2 carbene is electron rich and TFE is extremely electron deficient, there is the possibility of electron transfer (ET) to initiate an open-shell mechanism. Scheme 4-6 shows the calculated thermodynamics for ET. Disproportionation of two Co=CF_2 complexes via ET is endergonic by 53.2 kcal/mol. ET from Co=CF_2 to TFE requires 59.6 kcal/mol. Oxidation of the cobalt reactant species with O_2 requires 43.7 kcal/mol. All of these steps are higher in energy than C–C bond formation.

To analyze the effects of the fluorine substituents, the open-shell singlet mechanism with TFE was compared to the similar reaction mechanisms for ethylene and 1,1-difluoroethylene (DFE, Scheme 4-7). The barrier for C–C bond formation is 4.0 kcal/mol higher with ethylene compared to TFE and the resulting diradical intermediate is ~15 kcal/mol less stable. With DFE, the Co–$CF_2CF_2CH_2$• intermediate is 3.5 kcal/mol more stable than the alternative Co–

$CF_2CH_2CF_2$• isomer, but both are ~15 kcal/mol less stable compared to the perfluorinated intermediate. The preceding transition state barriers with DFE show a similar trend.

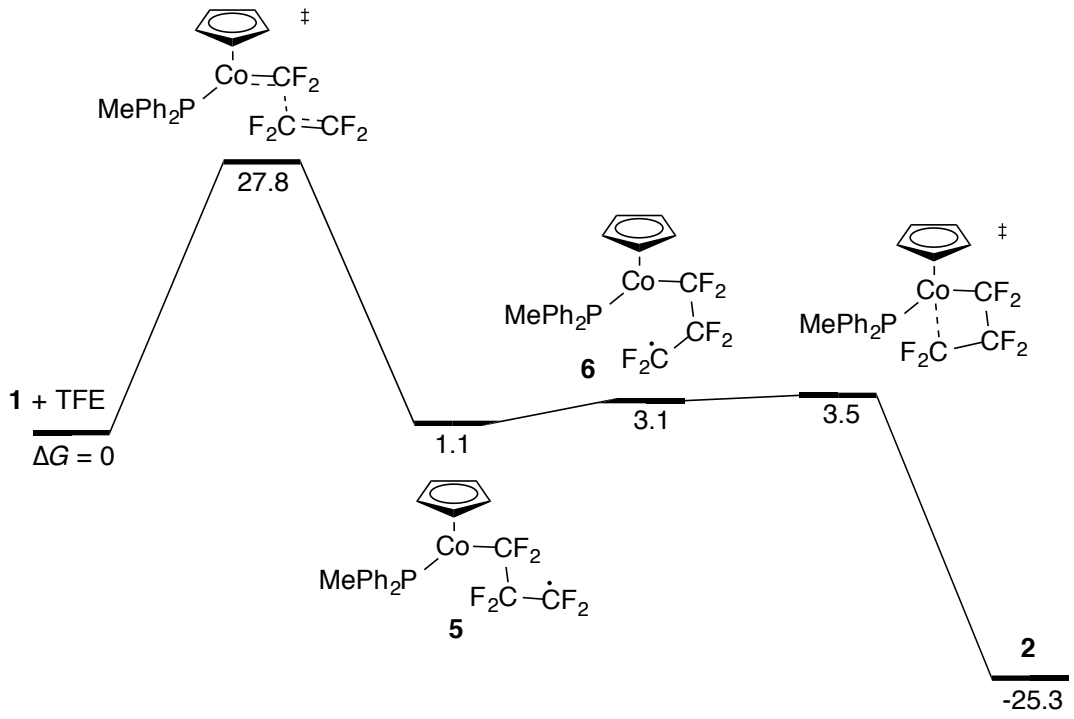

Scheme 4-5: Singlet free energy landscape for perfluorometallacyclobutane formation by C–C/Co–C stepwise cycloaddition (kcal/mol).

$$2\ Cp(PPh_2Me)Co{=}CF_2 \longrightarrow [Cp(PPh_2Me)Co{=}CF_2]^+ + [Cp(PPh_2Me)Co{=}CF_2]^- \qquad \Delta G = 53.2$$

$$Cp(PPh_2Me)Co{=}CF_2 + F_2C{=}CF_2 \longrightarrow [Cp(PPh_2Me)Co{=}CF_2]^+ + F_2C{=}CF_2^{\bullet -} \qquad \Delta G = 59.6$$

$$Cp(PPh_2Me)Co{=}CF_2 + O_2 \longrightarrow [Cp(PPh_2Me)Co{=}CF_2]^+ + O_2^{\bullet -} \qquad \Delta G = 43.7$$

Scheme 4-6: Electron transfer initiation steps for other potential mechanisms (kcal/mol).

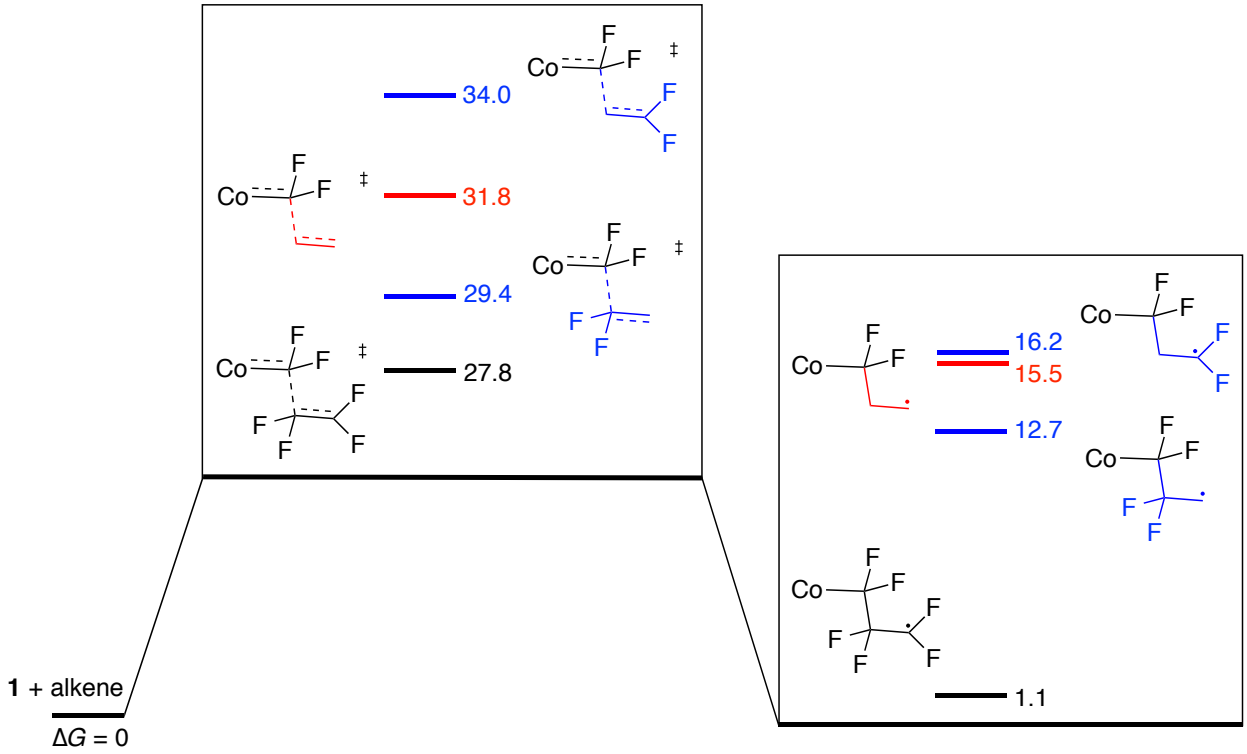

Scheme 4-7: Free Energies calculated for singlet diradical formation with TFE, DFE, and ethylene (kcal/mol).

Bent's rule provides, in part, a qualitative explanation for these calculated values.[20] Bent's rule suggests that polarization of bonds towards electronegative substituents causes these bonds to have greater p-character. This causes the other bonds to have greater s-character, which results in stronger bonds. TFE has a π-bond ~12 kcal/mol weaker than ethylene, which results in stabilization of the perfluoroalkyl intermediate. Also, for TFE and DFE, more CF_2–CF_2 bonds results in greater stability in the intermediates and transition states.

4.4 Conclusion

Calculations indicate that Cp(PPh_2Me)Co=CF_2 undergoes [2 + 2] cycloaddition with TFE by a unique open-shell singlet diradical mechanism, similar to the 1,4-diradical mechanism

found for organic cycloaddition reactions with TFE. The significant stability of the perfluorometallacyclobutane reveals why catalytic metathesis with TFE is difficult. This new mechanism will impact the future design of TFE metathesis catalysts.

4.5 References

1. Astruc, D. In *Olefin Metathesis: Theory and Practice*; Grela, K., Eds.; John Wiley & Sons, Inc.: Hoboken, New Jersey, 2014; pp 5–36.

2. Higman, C. S.; Lummiss, J. A. M.; Fogg, D. E. *Angew. Chem., Int. Ed.* **2016,** *55,* 3552–3565.

3. Deraedt, C.; d'Halluin, M.; Astruc, D. *Eur. J. Inorg. Chem.* **2013,** 4881–4908.

4. Nicolaou, K. C.; Bulger, P. G.; Sarlah, D. *Angew. Chem., Int. Ed.* **2005,** *44,* 4490–4527.

5. Fustero, S.; Simón-Fuentes, A.; Barrio, P.; Haufe, G. *Chem. Rev.* **2015,** *115,* 871–930.

6. Takahira, Y.; Morizawa, Y. *J. Am. Chem. Soc.* **2015,** *137,* 7031–7034.

7. Harrison, D. J.; Lee, G. M.; Leclerc, M. C.; Korobkov, I.; Baker, R. T. *J. Am. Chem. Soc.* **2013,** *135,* 18296–18299.

8. Frisch, M. J.; Trucks, G. W.; Schlegel, H. B.; Scuseria, G. E.: Robb, M. A.; Cheeseman, J. R.; Scalmani, G.; Barone, V.; Mennucci, B.; Petersson, G. A.; Nakatsuji, H.; Caricato, M.; Li, X.; Hratchian, H. P.; Izmaylov, A. F.; Bloino, J.; Zheng, G.; Sonnenberg, J. L.; Hada, M.; Ehara, M.; Toyota, K.; Fukuda, R.; Hasegawa, J.; Ishida, M.; Nakajima, T.; Honda, Y.; Kitao, O.; Nakai, H.; Vreven, T.; Montgomery, J. A., Jr.; Peralta, J. E.; Ogliaro, F.; Bearpark, M.; Heyd, J. J.; Brothers, E.; Kudin, K. N.; Staroverov, V. N.; Kobayashi, R.; Normand, J.; Raghavachari, K.; Rendell, A.; Burant, J. C.; Iyengar, S. S.; Tomasi, J.; Cossi, M.; Rega, N.; Millam, J. M.; Klene, M.; Knox, J. E.; Cross, J. B.; Bakken, V.; Adamo, C.; Jaramillo, J.; Gomperts, R.; Stratmann, R. E.; Yazyev, O.; Austin, A. J.; Cammi, R.; Pomelli, C.; Ochterski, J. W.; Martin, R. L.; Morokuma, K.; Zakrzewski, V. G.; Voth, G. A.; Salvador, P.; Dannenberg, J. J.; Dapprich, S.; Daniels, A. D.; Farkas, Ö.; Foresman, J. B.; Ortiz, J. V.; Cioslowski, J.; Fox, D. J. *Gaussian 09, Revision B.01*, Gaussian, Inc., Wallingford CT, USA, 2009.

9. Jaguar, versions 7.0–8.9, Schrödinger, LLC, New York, NY: 2007–2015.

10. Zhao, Y.; Truhlar, D. G. *Theor. Chem. Acc.* **2008,** *120,* 215–241.

11. a) Hariharan, P. C.; Pople, J. A. *Theor. Chim. Acta* **1973,** *28,* 213–222. b) Francl, M. M.; Pietro, W. J.; Hehre, W. J.; Binkley, J. S.; Gordon, M. S.; DeFrees, D. J.; Pople, J. A. *J. Chem. Phys.* **1982,** *77,* 3654–3665.

12. a) Hay, P. J.; Wadt, W. R. *J. Chem. Phys.* **1985,** *82,* 270–283. b) Hay, P. J.; Wadt, W. R. *J. Chem. Phys.* **1985,** *82,* 299–310.

13. a.) Weigend, F.; Ahlrichs, R. *Phys. Chem. Chem. Phys.* **2005,** *7,* 3297–3305. b.) Rappoport, D.; Furche, F. *J. Chem. Phys.* **2010,** *133,* No. 134105. c) Feller, D. *J. Comp. Chem.* **1996,** *17,* 1571–1586. d.) Schuchardt, K. L.; Didier, B. T.; Elsethagen, T.; Sun, L.; Gurumoorthi, V.; Chase, J.; Li, J.; Windus, T. L. *J. Chem. Inf. Model.* **2007,** *47,* 1045–1052.

14. a) Cortis, C. M.; Langlois, J. M.; Beachy, M. D.; Friesner, R. A. *J. Chem. Phys.* **1996,** *105,* 5472–5484. b) Cortis, C. M.; Friesner, R. A. *J. Comput. Chem.* **1997,** *18,* 1570–1590. c) Cortis, C. M.; Friesner, R. A. *J. Comput. Chem.* **1997,** *18,* 1591–1608.

15. Harvey, J. N.; Massimiliano, A.; Schwarz, H.; Koch, W. *Theor. Chim. Acc.* **1998,** *99,* 95–99.

16. Cramer, C. J. *Essentials of Computational Chemistry,* 2nd ed.; John Wiley & Sons: Chichester, England, 2004; pp 504–507.

17. http://www.chemcraftprog.com

18. Brothers, P. J.; Roper, W. R. *Chem. Rev.* **1988,** *88,* 1293–1326.

19. Gräfenstein, J.; Cremer, D. *Mol. Phys.* **2001,** *99,* 981–989.

20. Uneyama, K. *Organofluorine Chemistry*; Blackwell Publishing, Ltd: Oxford, U.K., 2006; pp 1–100.